EEET ECOLOGICAL ENGINEERING & ENVIRONMENTAL TECHNOLOGY

Ecological Engineering & Environmental Technology, 2026, 27(10), 306–331
https://doi.org/10.12912/27197050/231702
ISSN 2719–7050, License CC-BY 4.0

Received: 2026.08.03
Accepted: 2026.09.03
Published: 2026.09.10

An integrated approach for interpreting $PM_{2.5}$ composition and potential source characteristics in urban Tirana, Albania

Megi Caushaj[1*], Dhurata Premti[1], Hasime Manaj[1], Aferdita Shtembari[1], Glejdis Hajdini[2], Gloria Kosova[3]

[1] Department of Industrial Chemistry, Faculty of Sciences, University of Tirana, Albania
[2] Department of Chemistry, Faculty of Sciences, University of Elbasan, Albania
[3] Institute of Applied Nuclear Physics, Tirana, Albania
* Corresponding author's e-mail: megi_caushaj.fshnutdr@unitir.edu.al

ABSTRACT

Fine particulate matter ($PM_{2.5}$) is a complex atmospheric pollutant originating from multiple natural and anthropogenic sources. This pilot study investigates the chemical composition and potential source characteristics of $PM_{2.5}$ in urban Tirana, Albania, during two monitoring campaigns conducted in March–April 2024 and April–May 2025. Elemental composition was determined by energy-dispersive X-ray fluorescence (ED-XRF), while water-soluble non-purgeable organic carbon (NPOC) and total nitrogen (TN) were analyzed using a TOC-L analyzer. Pearson correlation analysis was applied to investigate relationships among $PM_{2.5}$ constituents, whereas MERRA-2 dust reanalysis, HYSPLIT backward trajectories, MODIS aerosol optical depth (AOD) and meteorological observations were used as complementary atmospheric information. The 2024 campaign was characterized by higher concentrations of crustal-associated elements and atmospheric conditions consistent with a relatively stronger mineral dust influence, whereas the 2025 campaign exhibited lower elemental concentrations and lower variability in crustal-associated elements. Moderate positive but statistically non-significant correlations between TN and NPOC were observed during both campaigns, consisting of partially shared atmospheric behavior. The combined interpretation of elemental composition, Pearson correlation analysis and complementary atmospheric datasets suggest that $PM_{2.5}$ composition reflects multiple potential source influences and atmospheric processing rather than a single dominant source. This integrated approach provides a practical qualitative framework for interpreting $PM_{2.5}$ composition in preliminary source assessment when quantitative receptor models are not available.

Keywords: $PM_{2.5}$, ED-XRF, pearson correlation analysis, HYSPLIT, MERRA-2, MODIS aerosol optical depth, non-purgeable organic carbon (NPOC), total nitrogen (TN), atmospheric transport, source interpretation.

INTRODUCTION

Atmospheric particulate matter (PM) consists of complex mixtures of solid and liquid particles suspended in the air. These particles may be emitted directly into the atmosphere as primary aerosols or formed through gas-to -particle conversion processes, resulting in secondary aerosols (Joutsensaari et al., 2018; Zhang et al., 2015; Zhang et al., 2012; Seinfeld and Pandis, 2016). The size distribution of airborne particles is highly heterogeneous, ranging from few nanometers to approximately 100 μm in arerodynamic diameter, depending on their sources and on the physical and chemical processes occurring in the atmosphere, such as condensation, coagulation, and chemical reactions (Thorpe and Harrison, 2008). Different PM fractions exhibit distinct physicochemical characteristics, atmospheric behavior, and health impacts, making particle size one of the most important parameters in air quality studies.

Among the different particulate matter fractions, fine particulate matter ($PM_{2.5}$), defined as airborne particles with an aerodynamic diameter smaller than 2.5 μm (Pan et al., 2022), is

recognized as one of the most important air pollutants affecting human health. Due to their small size, these particles can penetrate deeply into the respiratory system and reach the alveolar region of the lungs (Li et al., 2019). Numerous epidemiological studies have demonstrated significant associations between long-term $PM_{2.5}$ exposure and increased risks of cardiovascular and respiratory diseases, as well as premature mortality (Pope and Docker, 2006; Analitis et al., 2006; Zanobetti et al., 2009; Winterbottom et al., 2018).

$PM_{2.5}$ originates from a wide range of natural and antropogenic sources. Primary $PM_{2.5}$ is directly emitted into the atmosphere from source such as road traffic, industrial activities, biomass burning, fossil fuel combustion, sea spray, and resuspended soil dust (Streets et al., 2000). In addition, a substantial fraction of $PM_{2.5}$ may be formed secondarly through atmospheric chemical reactions (Kulmala, 2003; Griffith et al., 2013) involving gaseous precursors, including sulfur dioxide (SO_2) (Green et al, 2019), nitrogen oxides (NO_x) (Finlayson-Pitts et al., 2002; Zhang et al., 2015; Longfellow et al., 2000; Hu et al., 2023; Brown et al., 2006; Brown et al., 2016), ammonia (NH_3) (Zhang et al., 2015), and volatile organic compounds (VOCs) (Hallquist et al., 2009), leading to the formation of sulfate, nitrate and secondary organic aerosols. In urban environments, traffic emissions are often considered one of the major contributors to $PM_{2.5}$ concentrations through both exhaust and non-exhaust processes, including brake wear, tyre wear and road dust resuspension (Thorpe and Harrison, 2008; Grigoratos, and Martini, 2015). Natural sources such as mineral dust and marine aerosols may also significantly influence particulate matter composition, particularly in Mediterranean regions where long-range transport of Saharan dust and sea-salt particles frequently occures (Moreno et al., 2006; Pey et al., 2013). The relative importance of these sources varies according to local emission patterns, meteological conditions, and regional atmospheric transport processes. In addition to direct emissions, $PM_{2.5}$ composition is dynamically influenced by atmospheric transformation, regeneration and transport processes, which continuously modify the physical and chemical properties of aerosols during their atmospheric lifetime. Consequently, the chemical signatures measured at a reseptor site reflect not only local emission sources but also the cumulative effects of atmospheric processing and regional transport. Considering these processes is therefore essential for a more reliable interpretation of $PM_{2.5}$ chemical composition and source-related characteristics (Caushaj et al., 2026).

The chemical composition of $PM_{2.5}$ provides valuable information for understanding the origin and characteristics of airbone particles. In particular, elemental analysis has been widely used as an effective tool for source identification because specific elements can serve as tracers of different emission sources. Crustal materials are typically characterized by elevated concentrations of aluminum (Al), silicon (Si), calcium (Ca), zinc (Zn), and iron (Fe), which originate from brake wear, tyre wear, and road dust resuspension. Industrial and combustion-related sources may be identified through tracers including vanadiu (V), chromium (Cr), manganese (Mn), and arsenic (As), while sodium (Na), chloride (Cl) and magnesium (Mg) are commonly associated with marine aerosols and sea-salt particles (Moreno et al., 2006; Gietl et al., 2010; Grigortos and Martini, 2015; Amato et al., 2016). Consequently, the determination of the elemental composition represents an important approach for assessing the relative influence of natural and anthropogenic sources on $PM_{2.5}$ and for improving the understanding of urban air pollution dynamics.

The Mediterranean region is considered one of the most complex atmospheric environments in Europe due to the simultaneous influence of natural and anthropogenic emission sources. Air quality in this region is affected not only by local urban and industrial emissions but also by long-range transport processes, including the frequent intrusion of Saharan dust and the contribution of marine aerosols from Mediterranean Sea (Pey et al., 2013; Rodríguez et al., 2001; Escudero et al., 2007). Mineral dust transported from North Africa can substntially increase particulate matter concentrations and modify its chemical composition through the enrichment of crustal elements such as Al, Si, Ca, and Fe (Moreno et al., 2006). At the same time, sea-salt aerosols contribute characteristic marine tracers, including Na, Cl and Mg particulary in coastal and near-coastel areas (Putaud et al., 2004; Viena et al., 2008). In addition, rapid urbanization increasing traffic density and induastrial activities in many Mediterranean cities further enhance the complexity of $PM_{2.5}$ sources and atmospheric processes (Amato.et.al,2009). Consequently, understanding the chemical composition and source contributions of $PM_{2.5}$ in

Mediterranean urban environements remains essential for effective air quality manigment and the development of mitigation strategies.

Although air quality has become an increasing environmental concern in Albania, information regarding the chemical composition and source characteristics of $PM_{2.5}$ remains relatively limited. Recent research has highlighted the importance of aerosol pollution and its interaction with environmental and meteorological processes in the region, chemical characterization of $PM_{2.5}$ (Mandija et al., 2025; a.Caushaj et al., 2026; b.Caushaj et al., 2026). In addition, $PM_{2.5}$ has been recognized as an important carrier of chemical species with potential impacts on surrounding ecosystems (Premti et al., 2026). Recent GIS and remote-sensing studies have also documented ongoing land-use and land-cover changes in Albania and have highlighted the combined influence of land cover, vegetation, meteorological conditions, and anthropogenic factors on environmental conditions in the Tirana region (Çela et al., 2026; Papathimiu et al., 2026). Recent geospatial assessments of urban environmental conditions have likewise emphasized the importance of spatial variability and the interaction between urban structure, meteorological conditions, and anthropogenic pressures when evaluating environmental stress in densely populated cities (Ejaz et al., 2026). Evidence from other rapidly urbanized megacities has further shown that changes in anthropogenic activity can be reflected in urban environmental and air-quality conditions, as demonstrated during the COVID-19 lockdown in Karachi (Ali et al., 2024). As the largest urban center in the country, Tirana, While the analytical technique employed in this study, including XRF, water-soluble NPOC/TN analysis, Pearson correlation analysis, HYSPLIT backward trajectory modelling, MODIS Aerosol Optical Depth (AOD), and MERRA-2 aerosol reanalysis products, are individually well-established methods, their integrated application for $PM_{2.5}$ characterization and source interpretation has not previously been comprehensively reported for the urban environment of Tirana. To the best of our knowledge, studies in Albania addressing $PM_{2.5}$ chemical composition and source characteristics remain limited, particularly regarding the combined interpretation of chemical composition, statistical relationships among $PM_{2.5}$ constituents, and complementary atmospheric datasets. Therefore, the novelty of the present study lies not in the individual analytical techniques themselves, but in their integration within a single qualitative interpretation framework. Pearson correlation analysis was used to identify statistically associated $PM_{2.5}$ constituents, while HYSPLIT backward trajectories, MODIS AOD and MERRA-2 datasets were subsequently employed as complementary evidence to assess whether these statistical relationships were consistent with plausible atmospheric transport pathways and potential emission sources. Rather than replacing quantitative receptor models such as Positive Matrix Factorization (PMF), the integrated approach applied in this study is intended to provide a complementary framework for preliminary source characterization, particularly in regions where comprehensive long-term chemical characterization datasets and advanced source apportionment studies remain limited. Furthermore, this study contributes to an ongoing research effort aimed at progressively improving the understanding of $PM_{2.5}$ composition, atmospheric transformation processes, and source characteristics in Tirana through the integration of complementary chemical, statistical, and atmospheric analyses.

In this context the present study aimed to characterize the chemical composition of $PM_{2.5}$ collected at an urban site in Tirana, Albania, and to compare its temporal variability between two pilot monitoring campaigns conducted in 2024 and 2025. Particular emphasis was placed on identifying the potential contribution of crustal, traffic-related, industrial and marine sources based on elemental tracers determined by energy-dispersive X-ray fluorescence (ED-XRF). In addition, water-soluble non-purgeable organic carbon (NPOC) and total nitrogen (TN) were determined to further characterize the water-soluble organic and nitrogen fraction of $PM_{2.5.}$ The findings provide preliminary qualitative evidence on $PM_{2.5}$ chemical composition and potential source characterization, statistical relationships and complementary atmospheric datasets to support preliminary source interpretation in an urban environment.

MATERIALS AND METHODS

$PM_{2.5}$ sampling and gravimetric analysis

$PM_{2.5}$ samples were collected at an urban site in Tirana, Albania, in the vicinity of the Faculty of Natural Sciences, University of Tirana. Two

monitoring campaigns were conducted during March–April 2024 and April–May 2025 using a low-volume sampler (LVS6-RV) operated at a nominal flow rate of 2.3 $m^3\ h^{-1}$, in accordance with standard air-quality monitoring procedures (CEN, EN 12341:2014; Çaushaj et al., 2024). A total of nine $PM_{2.5}$ samples (S1–S9) were analyzed for the 2024 campaign and seven samples (S1–S7) for the 2025 campaign. Sampling was generally conducted over 24 h, and the actual sampled air volume was recorded for each sample. The LVS6-RV uses a temperature- and pressure-compensated flow-control system. According to the manufacturer specifications, the sampler provides controlled flow rates of 1.0, 2.3 and 3.0 $m^3\ h^{-1}$, with a deviation from the set point below 2%. The sampler had undergone calibration prior to use; however, a detailed calibration certificate and the associated calibration uncertainty were not available for the present study. Therefore, the documentation of flow performance was based on the manufacturer specifications and on the sample-specific air volumes recorded by the instrument during each sampling period. During sampling, the instrument records both the sampled air volume under ambient conditions and the normalized air volume (Nm^3), referenced to 273 K and 1013 mbar. Detailed information on sample identification, sampling dates, sampling duration, flow rate, sampled air volume and normalized air volume are provided in Tables 1 and 2.

$PM_{2.5}$ mass concentrations were determined gravimetrically from the difference between pre- and post-sampling filter masses. Filters were weighed under controlled laboratory conditions following equilibration prior to weighing. The balance readability was 0.1 mg; a formal measurement uncertainty was not independently established. Therefore, the gravimetric $PM_{2.5}$ concentrations should be interpreted with caution, particularly for samples with small filter mass differences approaching the practical resolution of the balance. In the present study, gravimetric $PM_{2.5}$ values are used primarily to describe concentration levels and temporal variability rather than as high-precision measurements. This limitation was taken into account when interpreting the relationships between $PM_{2.5}$ mass concentrations and the measured chemical constituents.

$PM_{2.5}$ samples were collected on polytetrafluoroethylene (PTFE) membrane filters (46.2 mm diameter, 2 µm pore size). Before and after sampling, the filters were conditioned under controlled laboratory conditions and weighed using an analytical balance After sampling, the filters were stored individually in sealed Petri dishes. The potential uncertainty associated with the gravimetric determination of $PM_{2.5}$ mass concentrations is addressed in the Study Limitations section.

The filters collected during March–April 2024 were stored for approximately 14–15 months prior to elemental and chemical analyses, which were carried out in June 2025 at the Institute of Atmospheric Science and Climate (ISAC-CNR), Lecce, Italy. Based on previous studies, this storage period is not expected to have substantially affected the elemental composition of the samples, as several of the investigated elements, including Al, Si, Fe, Ti, Cr, and Mn, are non-volatile and are generally considered stable on PTFE filters during long-term storage (U.S. EPA, 1999). Furthermore, previous studies on archived $PM_{2.5}$ filters have shown that particle-bound elements remain largely stable even after extended storage periods, with only minor variations observed (Hyslop et al., 2012). Therefore, although minor uncertainty associated with particle losses cannot be completely excluded, the elemental concentration

Table 1. Sampling information for $PM_{2.5}$ samples collected during the March–April 2024 monitoring campaign

Sample ID	Sampling date	Duration	Flow rate (m^3/h)	Sampled volume (m^3)	Normalized volume (Nm^3)
S1	27.03.2024	24h	2.3	55.2	54.49
S2	08.04.2024	24h	2.3	55.2	51.49
S3	12.04.2024	24h	2.3	55	51.65
S4	16.04.2024	24h	2.3	55.19	50.07
S5	19.04.2024	24h	2.3	55.2	51.5
S6	23.04.2024	24h	2.3	55.2	51.03
S7	25.04.2024	24h	2.3	54.76	50.08
S8	26.04.2024	24h	2.3	55.2	51.43
S9	30.04.2024	24h	2.3	55.2	50.53

Table 2. Sampling information for $PM_{2.5}$ samples collected during the April–May 2025 monitoring campaign

Sample ID	Sampling date	Duration	Flow rate (m³/h)	Sampled volume (m³)	Normalized volume (Nm³)
S1	17.04.2025	24h	2.3	55.19	51.31
S2	19.04.2025	24h	2.3	55.2	51.06
S3	21.04.2025	24h	2.3	55.18	50.75
S4	25.04.2025	24h	2.3	55.17	51.16
S5	27.04.2025	14h 45 min	2.3	33.9	31.16
S6	29.04.2025	24h	2.3	55.2	50.59
S7	01.05.2025	24h	2.3	55.19	50.46

patterns presented in this study are considered suitable for qualitative interpretation.

Elemental analysis by ED-XRF

Elemental concentrations were determined using a SPECTRO XEPOS05 energy-dispersive X-ray fluorescence (ED-XRF) spectrometer. Each filter was analyzed for 30 min, obtaining the concentrations of different elements after blank subtraction. The instrument was calibrated using 23 medium-concentration thin-film elemental standards (mass range between 6 and 50 μg/cm²; Micromatter Technologies Inc.). Measurements were performed according to the analytical procedure described by Unga et al. (2025). ED-XRF is a non-destructive technique that enables the direct determination of elemental surface loadings deposited on aerosol filters without chemical pretreatment.

The concentration of a specific element was quantified by subtracting the average value of the blank filters (M_β) from the ED-XRF measured value (M). In cases where the blank contribution was not measurable (< LOD), the corresponding analytical offset was added to M, whereas when $M < M_\beta$, one-half of the threshold value, defined as M_β plus its standard deviation (σ_β), was considered. All obtained data were subsequently divided by the PTFE calibration factor specific to each element. The resulting corrected surface loadings were subsequently converted to atmospheric elemental concentrations by accounting for the effective sampled filter area and the corresponding sample air volume. Final elemental concentrations were expressed in ng m^{-3} and represent the values used in the graphical and statistical analyses.

Quality assurance and quality control (QA/QC) procedures were implemented to assess the precision, reproducibility, and instrumental stability of the ED-XRF measurements. Replicate analyses were performed on selected samples and blanks, and the standard deviation of replicate measurements ranged from 0.21 to 5.34 ng cm^{-2}, depending on the element and its concentration level. The relatively low variability observed for most replicate measurements indicates satisfactory analytical repeatability. In addition, instrumental performance was evaluated through repeated measurements of elemental standards over the preceding 24 months. The relative standard deviation (RSD) values obtained for Fe, Ca, and S standards were 1.62%, 3.05%, and 1.48%, respectively, supporting satisfactory long-term instrumental stability and reproducibility of the ED-XRF measurements.

Element-specific method detection limits (MDLs) and uncertainty parameters were provided as part of the QA/QC information associated with the ED-XRF analytical procedure. For quantified elemental concentrations, analytical uncertainty was evaluated considering blank-filter variability (σB) and an element-specific proportional uncertainty parameter (h). Concentrations below the MDL or not distinguishable from blank variability were associated with an uncertainty of 100%. The element-specific MDLs and uncertainty parameters are reported in Table S1 (supplementary material). The same uncertainty framework and corresponding analytical parameters have also been reported in previous studies performed by the analytical research group using the same ED-XRF methodology (Potì et al., 2026).

The concentration of a specific species and sample was quantified if it was larger than the standard deviation σ_B of the blank filters; otherwise, a threshold value equal to $\sigma_B/2$ was considered. In cases in which the concentration was below the MDL, or not detectable above the average variability of the field blanks, a concentration value equal to the maximum between the MDL/2 and $\sigma_B/2$ was assumed. The uncertainty

for concentrations < MDL or not distinguishable from blanks were assumed to be 100%, whereas the uncertainty for quantified concentration, C_{ij}, of the sample i relative to the species j, was calculated as in (Potì et al., 2026) using the equation:

$$\Delta C_{i,j} = \frac{\sigma_{B,j}}{2} + h_j C_{i,j} \quad (1)$$

Extraction of the water-soluble fraction

The water-soluble fraction on $PM_{2.5}$ was obtained by placing each filter in 12 ml of ultrapure deionized water. Samples were subjected to ultrasonic extraction for 30 min at temperatures below 30 °C. The resulting extracts were filtered through 0.45 µm PTFE syringe filters prior to chemical analysis (Poti et al., 2026)

Determination of water-soluble NPOC and TN

Water-soluble non-purgeable organic carbon (NPOC) and total nitrogen (TN) were determined using a Shimadzu TOC-L analyzer following the analytical approach described by Pennetta et al. (2026). For NPOC determination, aliquots of the aqueous extracts were analyzed in NPOC mode following acidification with H_3PO_4 and sparging with purified air to remove inorganic carbon as CO_2 prior to analysis. An injection volume of 100 µL was used, with an acid addition of 1.4%, a sparge-gas flow of 101 mL min^{-1} and a sparging time of 44 s. Carbon-containing compounds were quantified following high-temperature catalytic oxidation at 720 °C and non-dispersive infrared (NDIR) detection of the generated CO_2. Total nitrogen was determined using the instrument's chemiluminescence detection system.

Instrument calibration was performed using certified standards, and the NPOC calibration covered the concentration range 0–10 mg L^{-1}, showing excellent linearity (R^2 = 0.9999). Sample extracts were analyzed using replicate injections according to the same instrumental procedure applied during calibration, and measurement variability was expressed as the standard deviation of the replicate measurements. Blank filters were analyzed to account for background contributions, and the mean blank concentrations were subtracted from the measured sample concentrations. Method detection limits (MDLs) of 30 ngC m^{-3} for NPOC and 50 ngN m^{-3} for TN were adopted based on the analytical methodology reported by Potì et al. (2026), where the corresponding values are reported for soluble organic carbon [(OC)s] and water-soluble total nitrogen (WSTN), respectively. The corresponding σB/2 values were 15 ngC m^{-3} for NPOC and 25 ngN m^{-3} for TN, with a proportional uncertainty parameter (h) of 0.05 for both measurements. For quantified concentrations, analytical uncertainty was evaluated as ΔCi,j = σB,j/2 + hjCi,j, where σB,j represents the standard deviation associated with blank-filter variability and hj is the proportional uncertainty parameter. For concentrations below the MDL or not distinguishable from blank variability, an uncertainty of 100% was assigned, following the same analytical framework reported by Potì et al. (2026). Final water-soluble NPOC and TN concentrations were calculated from the blank-corrected extract concentrations, the extraction volume (12 mL), and the corresponding sampled air volume and are reported in µg m^{-3}.

Data analysis

Elemental concentrations together with the water-soluble NPOC and TN concentrations were evaluated using descriptive statistical and graphical analyses. Samples collected during the 2024 and 2025 monitoring periods were compared to assess variability in $PM_{2.5}$ composition between the two monitoring campaigns. Pearson correlation analysis was performed to examine relationships among selected elemental tracers and between water-soluble NPOC and TN. For each evaluated elemental pair, the Pearson correlation coefficient (r), number of observations (n), p-value, and 95% confidence interval (CI) were calculated. Statistical significance was evaluated at $p < 0.05$. Given the limited number of samples (n = 9 in 2024 and n = 7 in 2025), the correlation analysis was used as an exploratory assessment of co-variation among $PM_{2.5}$ constituents rather than as evidence of common source origin. For the exceptionally strong correlations observed among crustal-associated elements in the 2024 dataset, an additional sensitivity analysis was performed after exclusion of the high-concentration S1 sample to evaluate its influence on the Pearson correlation coefficients. The interpretation of elemental relationships was based on tracers potentially associated with crustal, traffic-related, industrial, and marine influences, while recognizing that individual elements may originate from multiple sources.

COMPLEMENTARY ATMOSPHERIC DATASETS

To complement the chemical characterization of $PM_{2.5}$, additional atmospheric datasets were used to provide qualitative information on regional aerosol conditions and air-mass transport during the monitoring campaigns. Seventy-two-hour backward air-mass trajectories were generated using the NOAA Hybrid Single-Particle Lagrangian Integrated Trajectory (HYSPLIT) model with GDAS1 meteorological data, using the model vertical velocity option. Trajectories ended at 12:00 UTC at 500 m above ground level (AGL) at the sampling site (41.3351° N, 19.8158° E) (Stein et al., 2015).

For the evaluation of potential mineral-dust transport, the event-specific HYSPLIT analysis was not used to identify dust events independently. Instead, MERRA-2 Dust Surface Mass Concentration was used as an atmospheric indicator to identify distinct periods of enhanced dust loading within each monitoring campaign. For reproducibility, an episode was defined as a distinct local maximum in the hourly MERRA-2 Dust Surface Mass Concentration time series occurring during the monitoring period and clearly separated from adjacent values by a decline in dust concentration. The selected episodes corresponded to 27 and 29 March 2024 and 17 and 19 April 2025, for which individual 72-h backward trajectories were generated. Thus, four event-specific trajectories were evaluated in total.

HYSPLIT backward trajectories were subsequently used to characterize the preceding air-mass transport pathways and assess the geographical transport history of the air masses associated with these pre-defined episodes. Thus, the selection of trajectory dates was based on the MERRA-2 dust time series, whereas HYSPLIT was used to investigate whether the corresponding air-mass transport pathways were compatible with long-range transport from North Africa and the Mediterranean region. The trajectory interpretation was additionally compared with published reports of regional Saharan dust events occurring during the same periods. Agreement between enhanced MERRA-2 dust loading and transport pathways crossing potential dust-influenced regions was therefore treated as complementary evidence rather than as independent confirmation of dust occurrence or definitive source identification.

In parallel, campaign-wide transport patterns were assessed using 124 backward trajectories for each monitoring campaign, initiated at 6-h intervals throughout the respective sampling periods. These trajectory-frequency analyses were used to characterize the broader air-mass transport patterns reaching the study area during each campaign.

MERRA-2 M2T1NXAER v5.12.4 aerosol reanalysis data, with a spatial resolution of 0.5° × 0.625°, were used to examine hourly Dust Surface Mass Concentration and Sea Salt Surface Mass Concentration over the Tirana region *(Gelaro et al., 2017).* Regional aerosol loading was additionally evaluated using MODIS-Terra MOD08_D3 Collection 6.1 daily Aerosol Optical Depth (AOD) at 0.55 μm, with a spatial resolution of 1° × 1° *(Levy et al., 2017)*. MODIS AOD was considered as an indicator of total aerosol loading and not as direct evidence of a specific aerosol type.

Meteorological parameters, including air temperature, precipitation, relative humidity, wind speed, and incoming shortwave solar radiation, were obtained through the Open-Meteo Historical Weather API based on ERA5 reanalysis data (Hersbach et al., 2020) for a location representative of the sampling area (41.37° N, 19.78° E; 119 m a.s.l.). These atmospheric datasets were used as complementary environmental information and not for quantitative source apportionment or independent source identification.

The sampling site was located on the rooftop of Building B of the Faculty of Natural Sciences, in a central urban area of Tirana. The site is situated close to major road corridors and a busy road intersection characterized by continuous vehicle circulation throughout the day. In addition to traffic emissions, the surrounding area includes residential buildings, educational institutions, commercial activities, and other urban infrastructure typical of a densely populated city environment. As a result, the sampling location is exposed to a mixture of anthropogenic and natural emission sources, including traffic-related emissions, resuspended road dust, urban background pollution and regional atmospheric transport. The site was considered representative of urban air quality conditions in central Tirana and therefore suitable for investigating the chemical composition and source characteristics of $PM_{2.5}$. Measurements collected at this location provide valuable information for assessing the relative

influence of different emission sources and for improving the understanding of particulate matter pollution in the city.

RESULTS AND DISCUSSION

The chemical composition of $PM_{2.5}$ was investigated through elemental analysis and the determination of water-soluble non-purgeable organic carbon (NPOC) and total nitrogen (TN) in samples collected during the 2024 and 2025 monitoring campaigns. Sample-specific $PM_{2.5}$ mass concentrations and elemental concentrations for both campaigns are summarized in Tables S9 and S10. The elemental results were evaluated using source-related tracers reported in the literature and are discussed in relation to potential crustal, traffic-related, industrial and marine influences. Given the pilot nature of the study and the limited number of samples, the analysis focuses on concentration patterns, temporal variability and qualitative source-related characteristics rather than quantitative source apportionment. The $PM_{2.5}$ mass concentration reported in Tables S9 and S10 are subject to an important methodological limitation. Gravimetric filter weighing was performed using the available analytical balance, which did not provide the mass resolution required for high-precision gravimetric determination of particulate matter collected on filters. Consequently, $PM_{2.5}$ mass concentrations are associated with increased gravimetric uncertainty and are interpreted with caution. This limitation concerns the gravimetric $PM_{2.5}$ mass determination and does not directly affect the ED-XRF elemental concentrations reported in the same tables, which were obtained independently from the elemental signal measured on each filter, followed by blank correction, application of the element-specific PTFE calibration factors and normalization to the sampled air volume.

Figure 1 illustrates the distribution of crustal-associated elements during the two pilot sampling campaigns:

a) Silicon (Si) and calcium (Ca) were the dominant crustal elements in most samples, while aluminum (Al) and iron (Fe) also contributed substantially to the elemental composition. The predominance of these elements is commonly associated with crustal material and mineral dust sources (Moreno et al., 2006). Considerable variability was observed among the samples, with S1 exhibiting markedly higher concentrations of Al, S1, Ca and Fe compared with the remaining samples. Such enrichment of crustal tracers has been reported during periods of enhanced dust influence in Mediterranean environments (Moreno et al., 2006; Pey et al., 2013). The remaining samples showed lower concentrations, although crustal elements continued to represent an important fraction of $PM_{2.5}$ throughout the sampling period. Notably, Fe exhibited a strong co-variation with the typical crustal tracers Al, Si and Ca, particularly in sample S1, suggesting that its elevated concentration was largely influenced by mineral-rich dust. However, given the mixed origin of Fe, a contribution from traffic-induced road-dust resuspension cannot be excluded (Thorpe and Harrison, 2008).
b) The concentrations of crustal elements measured in $PM_{2.5}$ samples collected during 2025 are presented in Figure 1b. Si and Ca were the most abundant crustal elements, while Al and Fe also contributed substantially to the element profile. The highest crustal loadings were observed in samples S6 and S7, particularly for Ca, whereas S4 exhibited the lowest concentrations for most crustal tracers. Ti represents only a minor fraction of the measured crustal elements (Table 3).

A comparison of the 2024 and 2025 datasets revealed substantial differences in the concentrations and variability of crustal-associated elements. The 2024 samples showed markedly higher concentrations, particularly S1, with elevated Al, Si, Ca, and Fe, consistent with a stronger contribution of crustal material and mineral dust. In contrast, the 2025 dataset showed lower and more homogeneous concentrations, suggesting weaker crustal influence and more stable conditions. Nevertheless, both campaigns displayed similar elemental patterns, with Si and Ca among the predominant crustal-associated elements, consistent with contributions from mineral dust and resuspended soil particles, although elemental composition alone cannot quantitatively distinguish these sources.

The higher crustal tracer concentrations in 2024 may also reflect regional dust transport. Saharan dust intrusions were reported across the Mediterranean Basin and Balkan region during spring 2024 (EUMETSAT, 2024). Elevated Al, Si, Ca, and Fe, typical crustal tracers (Moreno et

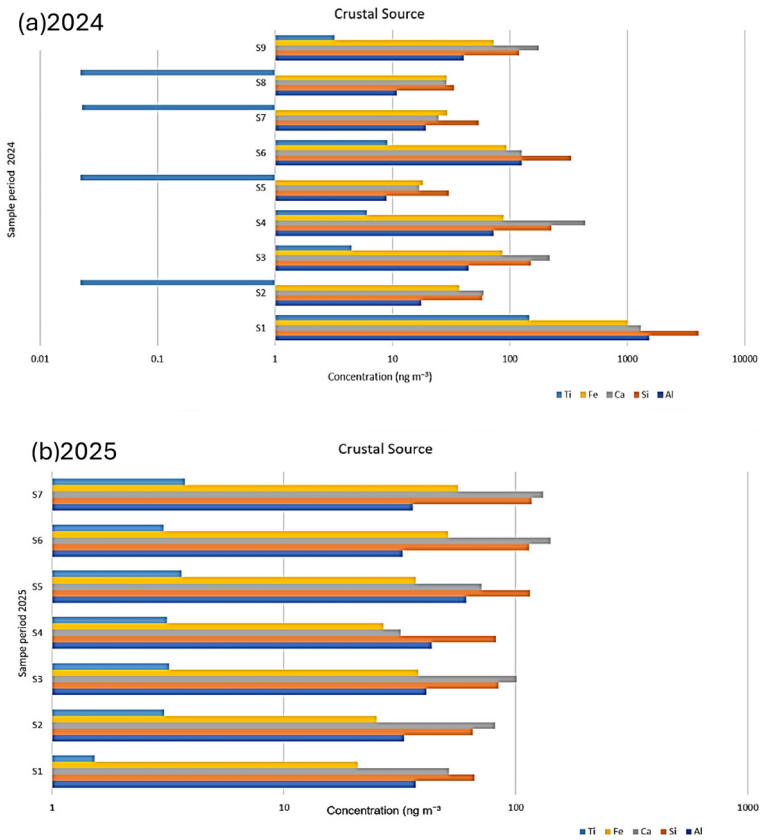

Figure 1. Concentrations of crustal-associated elements (Al, Si, Ca, Fe and Ti) in $PM_{2.5}$ samples collected during the 2024 (a) and 2025 (b) sampling campaigns. Concentrations are presented on a logarithmic scale (ng m^{-3})

Table 3. Maximum concentrations (ng/m^3) observed in 2024 and 2025

Element	Max 2024 (ng/m^3)	Max 2025 (ng/m^3)
Al	1531.87	61.04
Si	4039.09	117.25
Ca	1300.08	141.61
Fe	998.05	56.29

al., 2006), together with the reddish appearance of some filters, are consistent with a possible North African mineral dust influence. However, without back-trajectory or satellite-based dust tracking, Saharan dust cannot be conclusively confirmed and should be regarded as a plausible rather than definitive source attribution.

To complement the interpretation of the elemental concentration patterns, Pearson correlation analysis was performed to examine the relationships among the selected elemental tracers and chemical parameters. Strong positive correlations indicate similar temporal behavior among the analyzed species and may be consistent with common emission sources or shared atmospheric processes, whereas weaker correlations may reflect contributions from multiple sources or atmospheric transformations. (Çaushaj et al., 2024; Caushaj et al., 2026; Monod et al., 2000). In the present study, Pearson correlation analysis was not used as a standalone source apportionment method. Instead, the observed statistical relationships were interpreted together with elemental concentration patterns, established elemental source tracers reported in the literature, MERRA-2 dust reanalysis, HYSPLIT backward trajectory, MODIS (AOD) and meteorological observations. Therefore, the proposed source interpretation represents a qualitative interpretation based on the combined evaluation of chemical composition, statistical relationships, and complementary atmospheric datasets rather than on Pearson correlation analysis alone. Given the pilot nature of the study and the limited number of samples, the observed statistical relationships are intended to provide qualitative insight into $PM_{2.5}$ composition rather than definitive evidence of emission source contributions (Table 4).

The Pearson correlation analysis for the 2024 dataset revealed very strong positive correlations

among all crustal-associated elements (r = 0.95–1.00). Particularly high correlations were observed between Al, Si, Fe and Ti (r > 0.99), while Ca also exhibited strong relationship with the remaining elements. These statistical relationships are consistent with the observed concentration patterns and may reflect a similar temporal behavior among these crustal-associated elements during the March–April 2024 campaign. Compared with 2024 dataset, weaker and more variable correlations were observed in 2025. Strong positive correlations remained between Fe, Si and Ca (r = 0.87–0.88), whereas Al exhibited weaker associations with the other crustal tracers. Nevertheless, the observed relationships remain consistent with the contribution of crustal material to $PM_{2.5.}$

In the 2025 campaign, the correlation structure among crustal-associated elements was less pronounced than in 2024. Statistically significant positive correlations were observed for Si–Fe (r = 0.874, p = 0.010, 95% CI: 0.352–0.981) and Ca–Fe (r = 0.876, p = 0.010, 95% CI: 0.360–0.982), while other elemental pairs showed weak-to-strong correlations that did not reach statistical significance (p > 0.05), with confidence intervals including zero.

Overall, Pearson correlation analysis complements the elemental concentration patterns by describing co-variation among the measured constituents. Although stronger correlations among crustal-associated elements were observed in 2024 than in 2025, these relationships are interpreted cautiously given the limited sample size and the different sampling periods and meteorological conditions of the two campaigns. The exceptionally high coefficients observed in 2024 may partly reflect high-concentration observations within the dataset. Therefore, the correlations provide exploratory insight into elemental co-variation and atmospheric behavior rather than independent evidence of common source origin or changes in source intensity.

Additional sensitivity analyses were performed to assess the robustness of the exceptionally high 2024 correlations, including exclusion of the high-concentration S1 sample, leave-one-out and Spearman rank analyses, verification of the original sample-specific ED-XRF dataset and data-processing procedures, and visual assessment using scatter plots. These analyses confirmed that the strong Al–Si–Ti relationships were not solely attributable to S1; however, given the limited sample size, they are interpreted as patterns of consistent elemental co-variation rather than evidence of a common emission source. Detailed results are provided in the Supplementary Material (Tables S11–S14; Figures S1–S3).

MERRA-2 reanalysis indicated the presence of mineral dust over the study area during both monitoring campaigns. Dust concentrations were considerably higher and more variable during the 2024 period, with several pronounced peaks suggesting episodic increases in atmospheric dust loading. In contrast, the 2025 monitoring period exhibited substantially lower dust concentrations and more stable temporal pattern, indicating weaker mineral dust influence during sampling. Overall, the comparison indicates that mineral dust was present during both monitoring periods, although its atmospheric abundance was markedly greater in 2024 than in 2025.

Table 4. Pearson correlation coefficients among crustal-associated elements (Al, Si, Ca, Fe and Ti) measured in $PM_{2.5}$ samples during the 2024 and 2025 monitoring campaigns

2024	Al	Si	Ca	Fe	Ti
Al	1				
Si	0.9999	1			
Ca	0.9544	0.9569	1		
Fe	0.9986	0.9991	0.9642	1	
Ti	0.9998	0.9999	0.9568	0.9992	1
2025	Al	Si	Ca	Fe	Ti
Al	1				
Si	0.3294	1			
Ca	-0.4004	0.6132	1		
Fe	-0.1016	0.8735	0.8756	1	
Ti	0.3306	0.6756	0.4092	0.6405	1

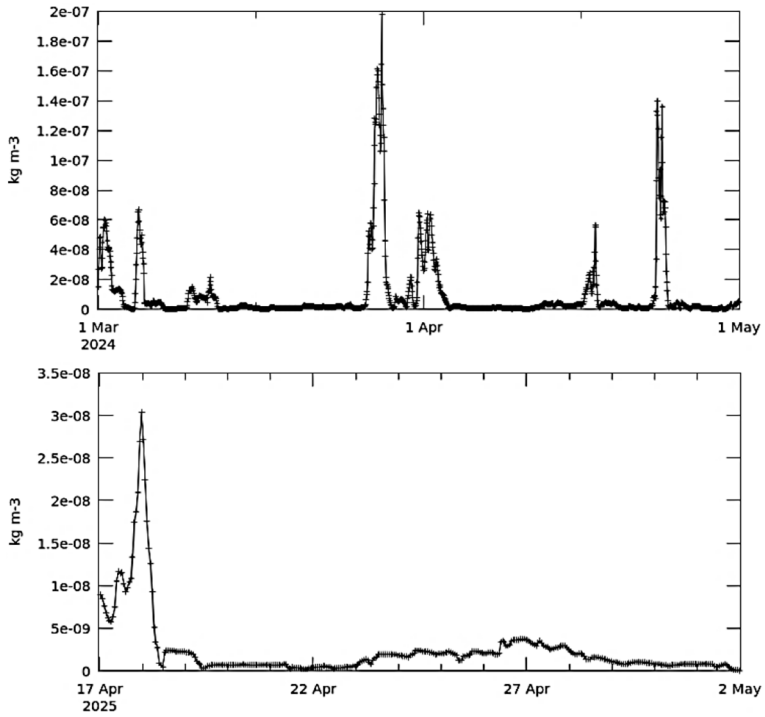

Figure 2. MERRA-2 dust surface mass concentration during the $PM_{2.5}$ sampling periods in 2024 and 2025

The 72-h HYSPLIT backward trajectories associated with the major dust peaks observed on 27 and 29 March 2024 (Figure 2) indicate that the air masses reaching Tirana followed long-range transport pathways from southern and southwestern sectors. The 27 March trajectory crossed North Africa and the central Mediterranean before reaching the receptor site, while the 29 March trajectory showed an extended pathway from the eastern Atlantic across North Africa and the Mediterranean basin toward Albania. These transport patterns are consistent with the potential long-range transport of mineral dust toward the study area during the 2024 campaign. When considered together with the pronounced MERRA-2 Dust Surface Mass Concentration peaks and elemental concentration patterns, the backward trajectories provide complementary atmospheric context for a possible contribution of regional and long-range mineral dust transport. In particular, the trajectories associated with the major dust peaks on 27 and 29 March 2024 are consistent with Saharan dust transport documented over the central Mediterranean during the same period (EUMETSAT, 2024; Pons et al., 2025). However, the trajectories alone do not confirm the origin of the transported air masses and should therefore be interpreted as complementary evidence rather than definitive source attribution (Figures 3–5).

The 72-h HYSPLIT backward trajectories associated with the main dust episode in 2025 indicate that the air masses reaching Tirana originated predominantly from the eastern and western Mediterranean regions, without a clear indication of long-range transport from North Africa. These transport pathways are consistent with the lower MERRA-2 dust surface mass concentration and the weaker correlations among the crustal-associated elements observed during the 2025 campaign, suggesting a relatively weaker influence of long-range mineral dust transport during the monitoring period.

The campaign-wide HYSPLIT frequency map, based on 124 backward trajectories, further shows that southern and southwestern transport pathways, including pathways extending across the Mediterranean toward North Africa, occurred during the 2024 monitoring period. These broader transport patterns are consistent with the pathways observed for the individual 27 and 29 March trajectories and indicate that air masses potentially influenced by North African regions could reach the study area on multiple occasions during the campaign. The combined evidence is consistent with a potential influence of long-range North African mineral dust on $PM_{2.5}$ composition during the 2024 campaign.

During the 2025 campaign, crustal-associated elemental relationships were weaker and

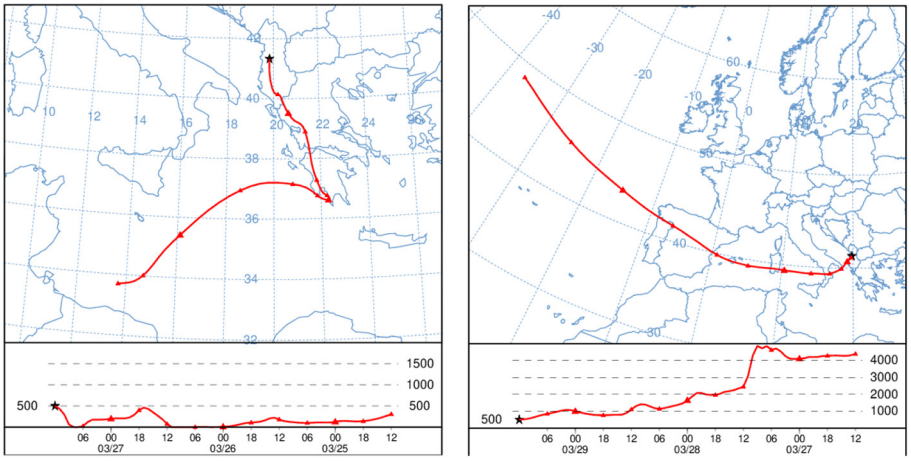

Figure 3. HYSPLIT 72-h backward trajectories (500 m AGL corresponding to selected periods of enhanced MERRA-2 dust surface mass concentration during the 2024 $PM_{2.5}$ monitoring campaign

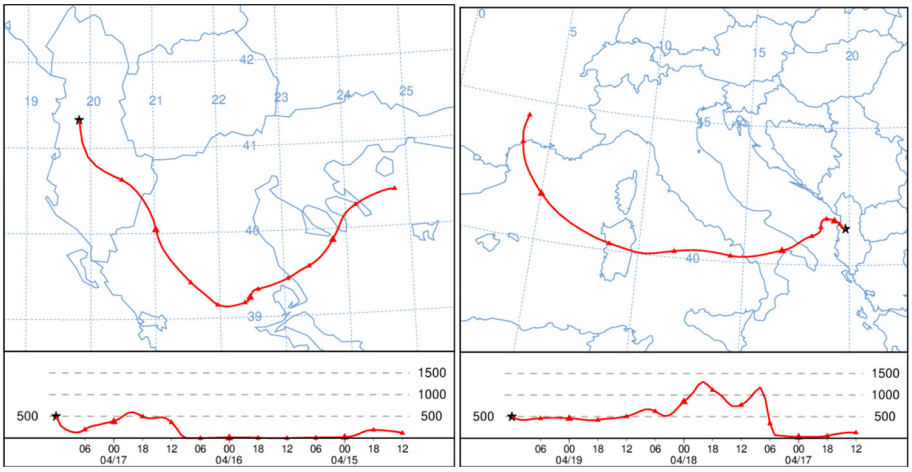

Figure 4. HYSPLIT 72-h backward trajectories (500 m AGL) correspond to the highest MERRA-2 dust surface mass concentration peaks during the 2025 $PM_{2.5}$ monitoring campaign

more heterogeneous than in 2024, with moderate correlations for Al–Si (r = 0.329) and Al–Ti (r = 0.331), and stronger associations for Si–Ti (r = 0.676), Si–Fe (r = 0.874), Ca–Fe (r = 0.876), and Fe–Ti (r = 0.641). The HYSPLIT frequency analysis showed broad air-mass pathways, including transport from continental Europe and southward and southwestward across the Mediterranean. Saharan dust transport across the central Mediterranean was independently documented immediately before the campaign; Sentinel-3 imagery on 15 April 2025 showed Saharan dust over the Mediterranean Sea and southern Italy transported northward by Sirocco winds (Copernicus, 2025). Thus, long-range North African mineral-dust transport was meteorologically plausible around the beginning of the campaign. However, the weaker crustal-element correlations and broader HYSPLIT pathways compared with 2024 do not support Saharan dust as a dominant source in 2025. Rather, the combined evidence is consistent with a possible intermittent contribution of long-range mineral dust superimposed on regional and continental crustal influences.

Overall, the HYSPLIT trajectory analysis complements the MERRA-2 reanalysis and the elemental composition results by providing additional atmospheric context for the qualitative interpretation of the observed $PM_{2.5}$ composition. While the 2024 campaign was characterized by transport pathways consistent with documented Saharan dust outbreaks over the central Mediterranean, the 2025 campaign was dominated by predominantly regional Mediterranean air masses and a comparatively weaker mineral dust signal.

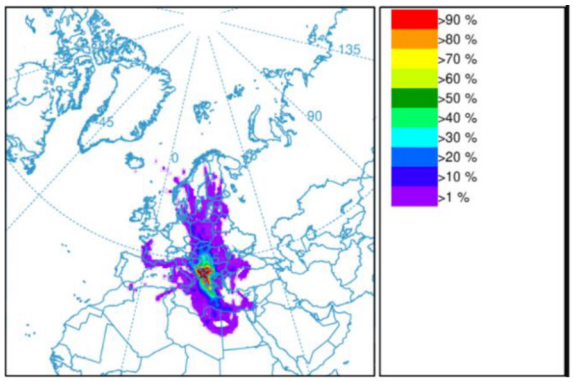

a)

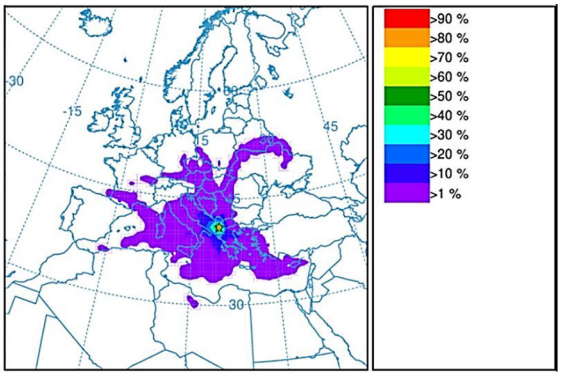

b)

Figure 5. HYSPLIT 72-h backward trajectory frequency maps for the $PM_{2.5}$ monitoring campaigns: (a) 2024 and (b) 2025. Each frequency analysis includes 124 backward trajectories initiated at 6-h intervals from the Tirana sampling site (41.3351° N, 19.8158° E), calculated at 500 m AGL using GDAS1 meteorological data

Taken together, these observations are consistent with a relatively greater influence of crustal material during the 2024 campaign than during the 2025 monitoring period.

MODIS AOD analysis provided additional regional aerosol context, with higher and more spatially extensive aerosol loading observed during the 2024 campaign than in 2025; the corresponding maps are provided in the Supplementary Material (Figure S4).

Among the analyzed elements (Figure 6), Fe exhibited the highest concentrations in all samples, with a pronounced peak in sample S1. Cu and Zn, commonly associated with tyre wear and brake wear (Pant and Harrison, 2013), showed moderate variability among the samples, whereas Cr and Mn were consistently present at lower concentrations. The occurrence of Fe together with Cu, Zn, Cr and Mn is consistent with the possible influence of non-exhaust traffic-related processes, including brake wear, tyre wear and traffic-induced road-dust resuspension (Amato et al., 2009; Thorpe and Harrison, 2008; Amato et al., 2014). However, because Fe also exhibited strong associations with the crustal tracers Al, Si and Ca, its elevated concentrations may reflect the combined influence of traffic-related processes, resuspended mineral-rich road dust and other crustal sources rather than a single emission source.

As in 2024, Fe exhibited the highest concentrations among the analyzed elements, although at considerably lower levels in 2025 (Figure 7) Zn and Cu, commonly associated with tyre and brake wear, respectively (Pant and Harrison, 2013), occurred at comparatively lower concentrations, while Cr and Mn also remained low. The co-occurrence of Fe, Cu, Zn, Cr, and Mn are consistent with the possible influence of non-exhaust traffic-related processes, including brake wear, tyre wear, and traffic-induced road-dust resuspension. However, Fe showed a concentration pattern comparable to the crustal-associated elements (Al, Si, and Ca), indicating that its elevated concentrations may reflect combined contributions from traffic-related processes, resuspended mineral-rich road dust, and other crustal sources rather than traffic emissions alone (Thorpe and Harrison, 2008; Moreno et al., 2006). Overall, the more homogeneous distribution of traffic-associated elements in 2025, together with the absence of statistically significant correlations among the selected tracers, is consistent with a less coherent traffic-related elemental pattern than in 2024 (Table 5).

The Pearson correlation analysis complements the interpretation of the observed elemental concentration patterns by examining the relationships among the selected traffic-related elements. In the 2024 dataset, only Fe, Cr and Mn exhibited very strong positive correlations ($r = 0.98–1.00$), whereas Zn and Cu showed weaker associations with the remaining tracers. In contrast, the 2025 dataset was characterized by generally weaker correlations, with no consistently associated group of elements. Overall, the observed relationships are consistent with the possibility that the selected traffic-related tracers may reflect contributions from multiple non-exhaust traffic-related processes rather than a single dominant emission source.

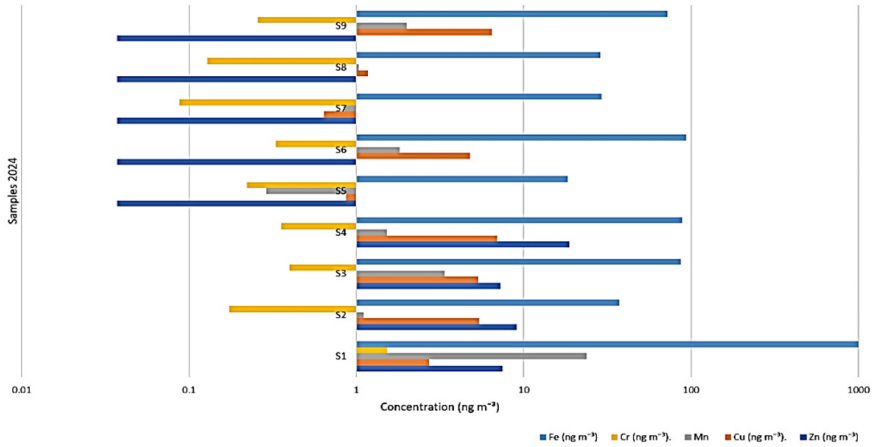

Figure 6. Concentrations of traffic-related elements (Fe, Cr, Mn, Cu and Zn) measured in $PM_{2.5}$ samples collected during March–April 2024

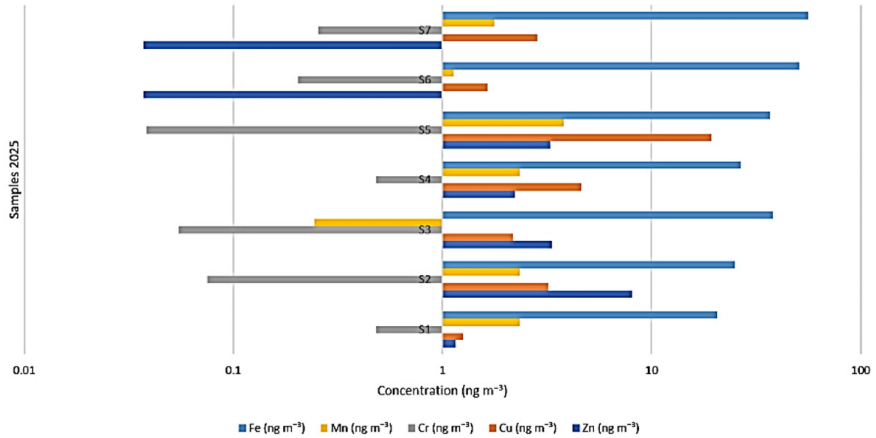

Figure 7. Concentration of traffic-related elements measured in $PM_{2.5}$ samples collected during April–May 2025

Industrial emissions are commonly associated with characteristic trace metals released from high-temperature industrial processes, metal production and manufacturing activities. Elemental tracers reported in the literature include Cr, Mn, Ni, Pb, Zn, V and As, although their relative abundance depends on the specific industrial activity (Pacyna and Pacyna, 2001; Querol et al., 2007; Amato et al., 2009). Cr, Mn and Ni have been associated with iron and steel production and metal-processing activities, whereas Zn and Pb have been associated with non-ferrous metallurgy, waste incineration and other industrial combustion processes (Pacyna and Pacyna, 2001; Querol et al., 2007). However, these elements are not source-specific and may also originate from other anthropogenic or natural processes. Therefore, the concurrent occurrence and similar temporal behavior of several industrial-related tracers may be consistent with a potential industrial influence but cannot by themselves provide definitive source attribution.

In the present study the selection of industrial tracers was constrained by the analytical capabilities of the ED-XRF system used for elemental determination. According to the laboratory analytical protocol, V, Ga, Zr, Te, I and Ba could not be quantified and were therefore excluded from the analysis. Consequently, the assessment of the industrial influence was based on Cr, Mn, Ni and Pb, which are recognized in the literature as representative tracers of industrial and metallurgical emissions (Thorpe and Harrison, 2008; Amato et al., 2009; Pant and Harrison, 2013). A more detailed statistical evaluation, including p-values and 95% confidence intervals, was also performed to further assess these relationships and is provided in the Supplementary Material (Tables S16–S16).

Table 5. Pearson correlation matrix for the selected traffic-related elemental tracers in $PM_{2.5}$ measured during the 2024 and 2025 monitoring periods

2024	Zn	Cu	Mn	Cr	Fe
Zn	1				
Cu	0.5867	1			
Mn	0.1815	-0.0904	1		
Cr	0.2627	0.0071	0.9854	1	
Fe	0.1934	-0.0891	0.9974	0.9866	1
2025	Zn	Cu	Cr	Mn	Fe
Zn	1				
Cu	0.1677	1			
Cr	-0.489	-0.4047	1		
Mn	0.2156	0.7501	0.076	1	
Fe	-0.5487	-0.0102	-0.319	-0.349	1

At Figure 8 Mn showed the highest concentration among the industrial tracers, particularly in S1, while Pb was moderate and Cr and Ni remained comparatively low. The absence of concurrent enrichment in Cr, Mn, Ni, and Pb is consistent with no clear evidence of a dominant industrial contribution during the 2024 campaign. Occasional enrichment of individual elements may reflect localized or intermittent industrial activities, although other natural and anthropogenic sources cannot be excluded (Querol et al., 2007; Pacyna and Pacyna, 2001).

As in the 2024 campaign, the selected industrial-related elements did not exhibit a consistent enrichment pattern across the analyzed samples. The concentrations of the individual elements varied among samples without a common temporal trend, indicating that the selected industrial tracers were not simultaneously enriched during the sampling period. Compared with the 2024 dataset, the concentrations were generally lower and more homogeneous, which is consistent with the absence of a clear enrichment pattern among the analyzed industrial tracers during the 2025 monitoring campaign (Querol et al., 2007). Consequently, no clear evidence of a dominant industrial contribution was identified among the elemental tracers analyzed during the 2025 campaign (Figure 9, Table 6).

During the 2024 campaign, Cr–Mn showed a very strong positive correlation (r = 0.985), while Ni was weakly correlated with Cr (r = 0.167) and Mn (r = 0.076), and Pb showed moderate correlations with Ni (r = 0.671), Cr (r = 0.414), and Mn (r = 0.361). Overall, the industrial-related elements did not exhibit consistently strong correlations or common temporal behavior, consistent with the concentration profiles in Figure 7, where no simultaneous enrichment of all analyzed industrial tracers was observed. Given the pilot nature of the

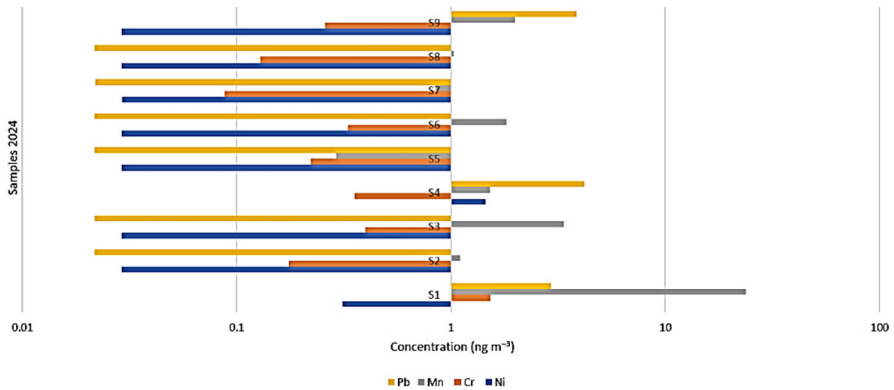

Figure 8. Concentrations of the selected industrial-related elements (Cr, Mn, Ni and Pb) measured in $PM_{2.5}$ samples collected during the 2024 sampling campaign

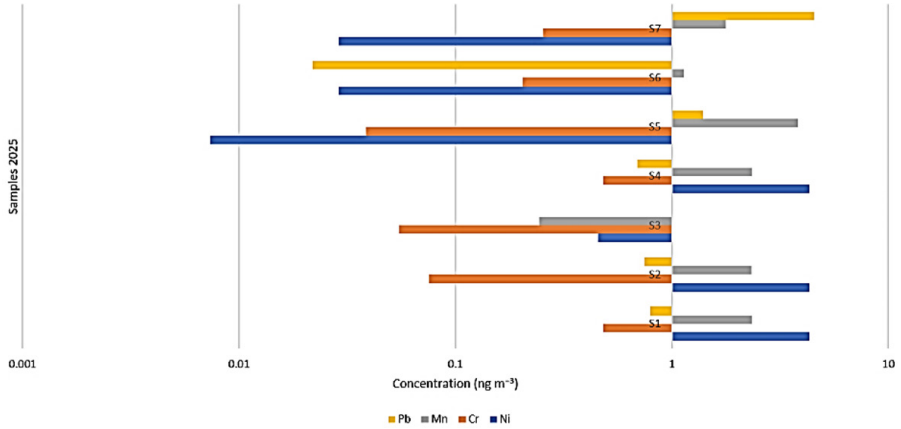

Figure 9. Concentrations of the selected industrial-related elements (Cr, Mn, Ni and Pb) measured in $PM_{2.5}$ samples collected during the 2025 sampling campaign

Table 6. Pearson correlation coefficients among the selected industrial-related elements (Ni, Cr, Mn and Pb) measured in $PM_{2.5}$ samples collected during the 2024 and 2025 monitoring campaigns

Year 2024	Ni	Cr	Mn	Pb
Ni	1			
Cr	0.167	1		
Mn	0.076	0.985	1	
Pb	0.671	0.414	0.361	1
Year 2025	Ni	Cr	Mn	Pb
Ni	1			
Cr	0.568	1		
Mn	0.241	0.076	1	
Pb	-0.373	-0.027	0.05	1

study and limited sample size, these correlations are interpreted as exploratory statistical relationships and considered together with the elemental concentration patterns rather than as independent evidence of common emission sources.

In 2025, correlations were generally weaker, with the strongest positive relationship between Ni–Cr (r = 0.568). Mn showed very weak correlations with the remaining elements (r = 0.05–0.24), while Pb exhibited negligible or negative correlations, including a moderate negative correlation with Ni (r = −0.373). The absence of consistently strong positive correlations, together with the relatively homogeneous concentration profiles in Figure 8, is consistent with no clear common enrichment pattern among the industrial-related tracers during the 2025 campaign. Additional analysis using p-values and 95% confidence intervals was performed to assess the statistical significance and uncertainty of these relationships and is provided in the Supplementary Material (Tables S17–S18).

At Figures 10, 11; Na, Cl, and Mg showed considerable variability, with the highest Na and Cl concentrations in S4, while S1 exhibited elevated Mg together with relatively high Na and Cl. Although commonly associated with marine aerosols, these elements may also have natural and anthropogenic sources; in particular, elevated Mg in S1 may reflect both marine and mineral-rich crustal influences (Querol et al., 2007; Vicars and Sickman, 2011). Given Tirana's location approximately 30 km from the Adriatic coast, these concentrations are consistent with a possible marine influence under favorable meteorological conditions, as reported for other Mediterranean urban environments (Pey et al., 2013). However, elemental composition alone cannot unambiguously distinguish marine from non-marine sources, and the substantially lower concentrations in the remaining samples are consistent with an intermittent rather than persistent marine influence during the 2024 campaign.

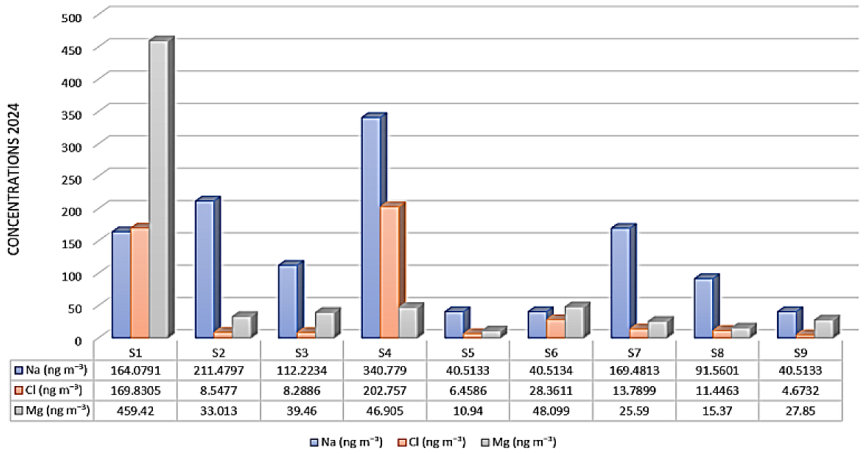

	S1	S2	S3	S4	S5	S6	S7	S8	S9
Na (ng m^{-3})	164.0791	211.4797	112.2234	340.779	40.5133	40.5134	169.4813	91.5601	40.5133
Cl (ng m^{-3})	169.8305	8.5477	8.2886	202.757	6.4586	28.3611	13.7899	11.4463	4.6732
Mg (ng m^{-3})	459.42	33.013	39.46	46.905	10.94	48.099	25.59	15.37	27.85

Figure 10. Distribution of marine-associated elements (Na, Cl and Mg) in $PM_{2.5}$ samples collected during the March–April 2024 monitoring period

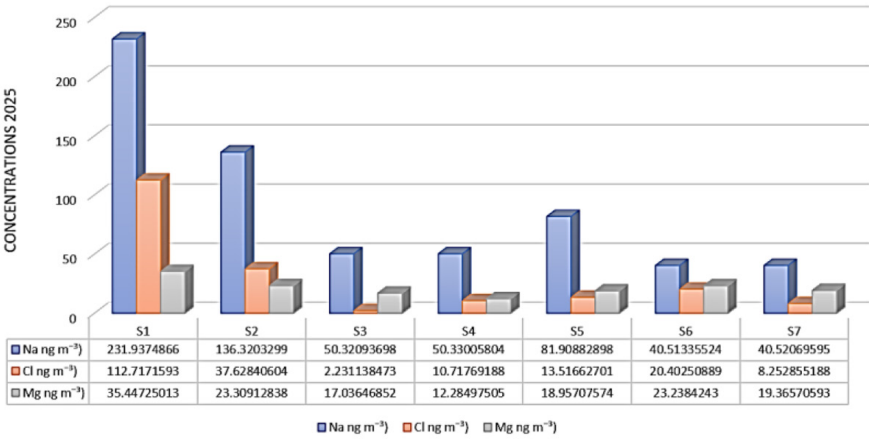

	S1	S2	S3	S4	S5	S6	S7
Na ng m^{-3})	231.9374866	136.3203299	50.32093698	50.33005804	81.90882898	40.51335524	40.52069595
Cl ng m^{-3})	112.7171593	37.62840604	2.231138473	10.71769188	13.51662701	20.40250889	8.252855188
Mg ng m^{-3})	35.44725013	23.30912838	17.03646852	12.28497505	18.95707574	23.2384243	19.36570593

Figure 11. Concentrations of marine-related elements measured in $PM_{2.5}$ samples collected during April–May 2025

Na remained the dominant marine-associated element, with the highest concentration observed in sample S1, followed by S2. Cl exhibited a similar concentration pattern, whereas Mg showed lower concentrations and less variability among the samples. The relatively higher Na and Cl concentrations observed in S1 and S2 are consistent with a possible marine influence, although these elements may also originate from additional natural and anthropogenic sources.

Compared with the 2024 dataset, the 2025 samples exhibited generally lower concentrations and a more homogeneous distribution of the analyzed marine-associated elements, without the pronounced concentration peaks observed previously. These observations are consistent with reduced variability in the analyzed marine-associated elements during the 2025 monitoring campaign and may also reflect differences in meteorological conditions and regional air-mass transport. Overall, the observed elemental patterns suggest that marine influence was intermittent during both monitoring campaigns, with comparatively higher Na and Cl concentrations observed during the 2024 campaign. However, the elemental composition alone does not allow an unambiguous distinction between marine and non-marine sources (Table 7).

The Pearson correlation analysis complements the interpretation of the observed concentration patterns by examining the relationships among the selected marine-associated elements. In the 2024 dataset, a moderate positive correlation was observed between Na and Cl ($r = 0.70$), whereas Mg exhibited weak correlations with both Na and Cl, indicating that its temporal variability may have been influenced by additional natural or anthropogenic sources besides marine

aerosols. In contrast, the 2025 dataset was characterized by strong positive correlations among Na, Cl and Mg (r = 0.85–0.95), indicating a more similar temporal behavior among these elements during the monitoring period.

Additional statistical and quantitative analyses were performed to further evaluate the marine-associated tracers. Pearson correlations were assessed using p-values and 95% confidence intervals (Table S19), showing a significant Na–Cl correlation in 2024 and significant correlations among Na, Cl, and Mg in 2025. Cl-based sea-salt concentrations and approximate $PM_{2.5}$ sea-salt fractions were also estimated (Table S20), ranging from approximately 8.4–365.0 ng m^{-3} (0.02–1.73%) in 2024 and 4.0–202.9 ng m^{-3} (0.08–2.80%) in 2025. Overall, these estimates do not indicate a dominant sea-salt contribution to $PM_{2.5}$ during either monitoring campaign. However, these fractions represent approximate estimates rather than precise quantitative source contributions, because formal uncertainty for the gravimetric $PM_{2.5}$ mass determination was not established, and the balance resolution limits the precision of the measured filter-mass differences. Furthermore, Cl-based reconstruction may underestimate atmospherically aged sea-salt aerosol because particulate chloride can be depleted during atmospheric transport through heterogeneous reactions with acidic species (Su et al., 2022). Therefore, the relatively low Cl-based estimates do not demonstrate the absence of a marine contribution. When considered together with the observed Na–Cl–Mg relationships and the complementary atmospheric datasets, the results indicate that a dominant marine contribution is not supported, while a possible intermittent marine influence cannot be excluded (Figures 12, 13).

Table 7. Pearson correlation matrix of marine-associated elements (Na, Cl and Mg) measured in $PM_{2.5}$ samples during the 2024 and 2025 monitoring periods

2024	Na	Cl	Mg
Na	1		
Cl	0.7029	1	
Mg	0.1482	0.6118	1
2025	Na	Cl	Mg
Na	1		
Cl	0.9524	1	
Mg	0.8530	0.9187	1

MERRA-2 reanalysis indicated the presence of sea-salt aerosols over the study area during both monitoring periods. Although the temporal variability differed between the two campaigns, the reanalysis suggests that marine aerosols were present in the regional atmosphere throughout the sampling periods.

The HYSPLIT backward-trajectory frequency analysis for the 2024 monitoring campaign was based on 62 individual 72-h backward trajectories generated at 500 m AGL using GDAS1 meteorological data. The resulting frequency map indicates that air masses reaching the receptor site frequently travelled over the Adriatic Sea and the central Mediterranean before arriving in Tirana. These transport pathways are consistent with the possible transport of marine air masses toward the study area during the $PM_{2.5}$ sampling period. Similarly, the 2025 backward trajectory frequency map shows that air masses also reached the receptor site through pathways crossing the Adriatic and Mediterranean regions, although a greater influence of continental transport from central Europe was also observed. These transport patterns indicate that both marine and continental air masses affected the study area during the 2025 monitoring campaign.

Comparison of the two monitoring campaigns indicates that transport pathways crossing marine regions were present during both sampling periods. While the 2024 campaign was characterized by a relatively greater influence of trajectories crossing the central Mediterranean, the 2025 campaign exhibited a comparatively stronger continental component together with persistent transport over the Adriatic Sea.

When considered together, the MERRA-2 Sea-Salt Surface Mass Concentration reanalysis, HYSPLIT backward trajectory analysis, Pearson correlation analysis and the elemental concentration patterns provide complementary atmospheric information for the qualitative interpretation of a possible marine influence on the $PM_{2.5}$ composition during both monitoring campaigns. Although none of these approaches independently distinguishes marine from non-marine sources, their combined interpretation is consistent with intermittent marine influence under favorable atmospheric transport conditions.

NPOC concentrations were consistently higher than TN throughout the sampling period, with a pronounced peak observed in sample S4. In contrast, TN exhibited more moderate variability

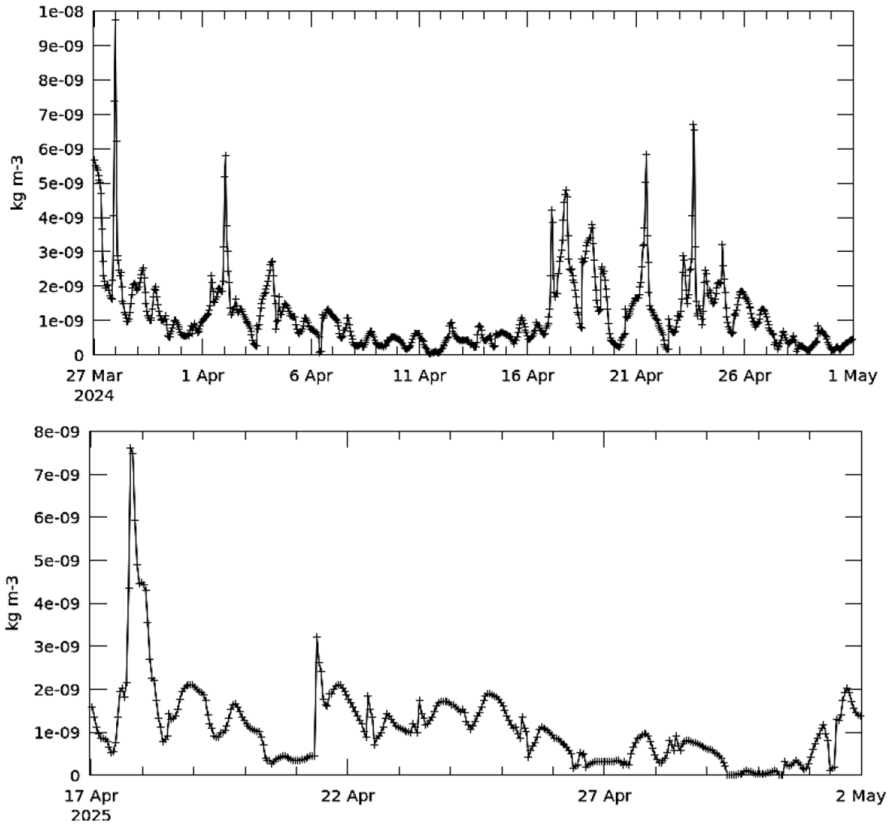

Figure 12. MERRA-2 sea salt surface mass concentration over the study area during the 2024 (27 March–30 April 2024) and 2025 (17 April–1May 2025) monitoring campaigns

among the samples. The elevated NPOC concentration observed in S4 indicates a period of increased organic carbon in $PM_{2.5}$ relative to the remaining samples. Although this observation may reflect enhanced secondary organic aerosol formation or the influence of localized emission sources, the available dataset does not allow these potential processes to be distinguished. The remaining samples exhibited comparatively lower NPOC concentrations and less pronounced temporal variability. (Figure 14)

Like the 2024 dataset, NPOC concentrations remained consistently higher than TN in all samples. However, both parameters exhibited a more gradual and homogeneous temporal variation, without the pronounced peak observed in 2024. The similar temporal patterns of NPOC and TN observed during the 2025 monitoring campaign are consistent with comparatively lower temporal variability than that observed in 2024. Although these observations may reflect differences in atmospheric processes or emission conditions, the available dataset does not allow the underlying causes of these variations to be distinguished. (Figure 15, Table 8)

The Pearson correlation analysis revealed a moderate positive correlation between TN and NPOC during both monitoring periods ($r = 0.645$ in 2024 and $r = 0.650$ in 2025). The similar correlation coefficients observed in both datasets indicate a consistent temporal relationship between the two parameters. These observations are consistent with partially shared atmospheric behavior; however, the observed correlations may also reflect the influence of $PM_{2.5}$ mass, meteorological conditions and multiple atmospheric processes rather than a single common source (Caushaj et al., 2026; Pey et al., 2013).

A similar NPOC–TN relationship was observed during the two monitoring campaigns, with moderate positive correlations in both 2024 ($r = 0.640$, $p = 0.061$) and 2025 ($r = 0.650$, $p = 0.114$). Neither correlation was statistically significant, indicating the absence of a strong and statistically supported association between the two components. The consistent moderate but non-significant relationships across both campaigns may reflect contributions from different sources or atmospheric processes rather than a single dominant common source (Table S21).

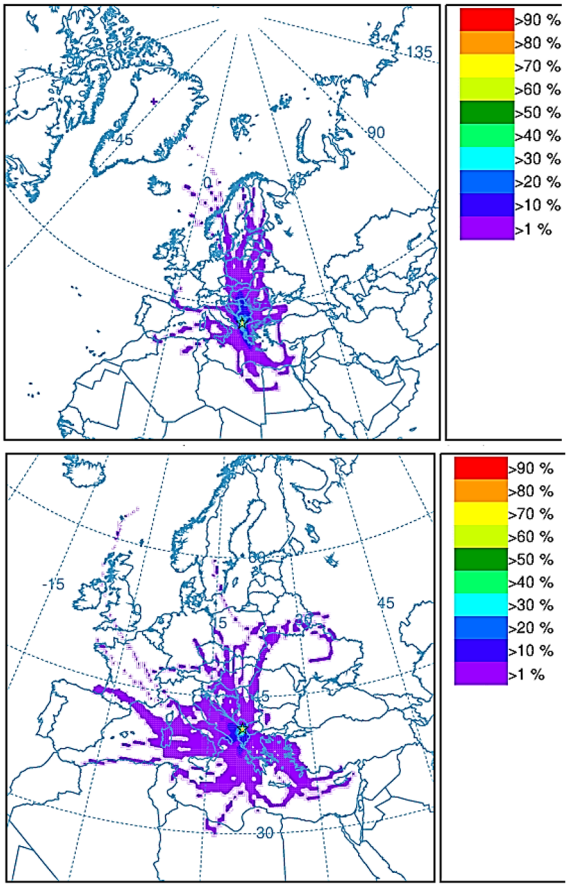

Figure 13. NOAA HYSPLIT 72-h backward trajectory frequency maps (500 m AGL) for 2024 (27 March–30 April) and 2025 (17 April–1 May2025) $PM_{2.5}$ monitoring campaigns

Previous studies have applied correlation analysis to atmospheric pollutants, particularly gaseous species, to explore relationships among measured pollutants and their potential association with common emission processes (Monod et al., 2000; c.Çaushaj et al., 2024). In the present pilot study, a similar exploration approach was applied to the chemical constituents of $PM_{2.5}$. Pearson correlation analysis was used to examine whether elemental and chemical constituents within the $PM_{2.5}$ fraction exhibited similar temporal behavior, while source-related interpretations were made cautiously and in combination with the observed concentration patterns and complementary atmospheric information.

The different correlation patterns observed among crustal-, traffic-, marine- and industrial-associated tracers suggest heterogeneous behavior among the measured $PM_{2.5}$ constituents. Rather than representing distinct source signatures, these patterns are consistent with the complex nature of atmospheric particulate matter, in which individual constituents may originate from multiple sources and may also be affected by atmospheric transport and transformation processes. This interpretation is consistent with the conceptual framework proposed by c.Caushaj et al. (2026), which describes atmospheric particulate matter as a dynamic system continuously modified by emission, transport, transformation and regeneration processes. Under this framework, the chemical composition measured at the receptor site can be regarded as the cumulative result of interacting atmospheric processes rather than as a direct fingerprint of a single emission source. Accordingly, the relationships among the measured $PM_{2.5}$ constituents are interpreted here as part of an integrated qualitative assessment rather than as quantitative source apportionment. To provide additional environmental context for the differences observed between the two monitoring campaigns, the principal meteorological parameters were subsequently evaluated throughout both sampling periods.

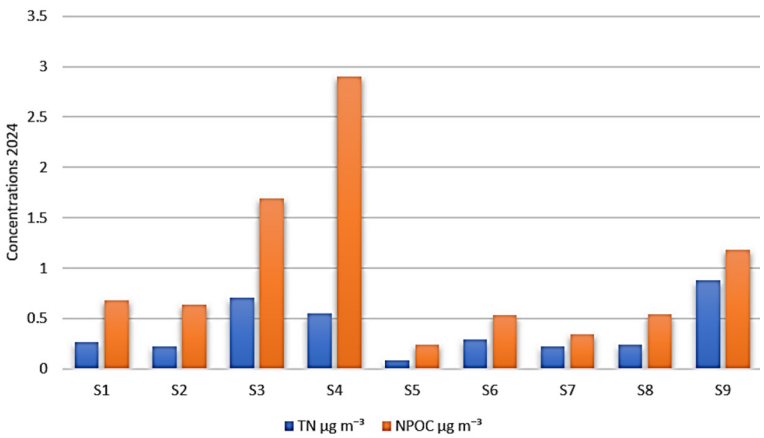

Figure 14. Variation of NPOC and TN concentrations (µg/m³) across the analyzed filters 2024

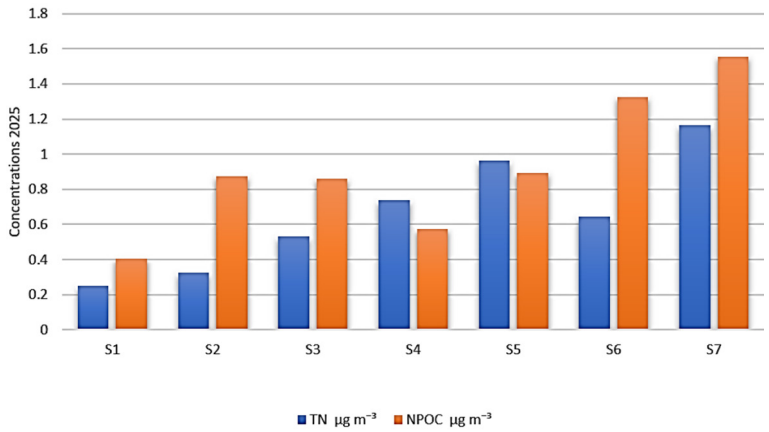

Figure 15. Variation of NPOC and TN concentrations (µg/m³) across the analyzed filters 2025

Table 8. Pearson correlation coefficients between TN and NPOC measured in $PM_{2.5}$ samples during the 2024 and 2025 monitoring periods

2024	TN	NPOC
TN	1	
NPOC	0.6448	1
2025	TN	NPOC
TN	1	
NPOC	0.6502	1

The comparison of the mean meteorological conditions provides additional environmental context for interpreting the differences observed between the two monitoring campaigns. The 2024 campaign was characterized by greater overall meteorological variability, whereas 2025 exhibited generally more stable and drier conditions (Figure 16). These differences indicate that the two monitoring periods occurred under distinct meteorological conditions, which may affect aerosol dispersion, transport, residence time, wet removal and physicochemical processing. Precipitation can remove suspended particles through wet scavenging, while relative humidity can influence water uptake, hygroscopic growth, coagulation and deposition, and wind conditions can affect aerosol dispersion and transport (Wei-wei, 2009; Gaffney and Marley, 2005; Tomasi and Lupi, 2017). In the present study, however, these meteorological parameters were evaluated descriptively and are therefore considered as environmental context rather than as evidence of direct causal effects on the observed $PM_{2.5}$ composition.

The meteorological context is also relevant to the interpretation of TN and NPOC. The moderate positive correlation observed between these parameters ($r \approx 0.65$ in both campaigns) is consistent with partially shared atmospheric behavior; however, it may also reflect their dependence on $PM_{2.5}$ mass, meteorological conditions or multiple atmospheric processes rather than a single common source. Processes such as atmospheric transport, oxidation, gas–particle partitioning and aqueous-phase reactions can modify organic- and nitrogen-containing aerosol fractions during

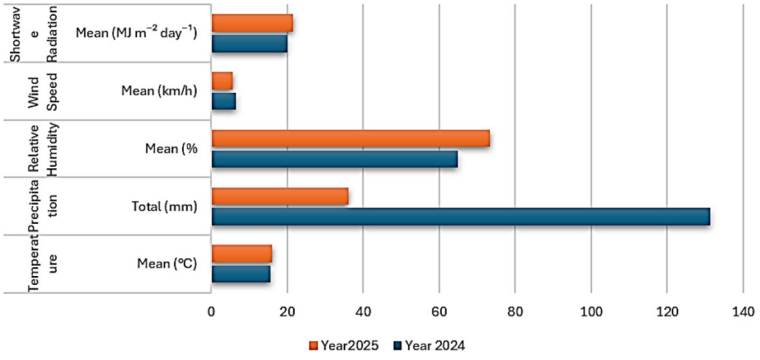

Figure 16. Comparison of mean meteorological conditions during the 2024 and 2025 campaigns

atmospheric residence (Hallquist et al., 2009; Ervens et al., 2011). Accordingly, the observed TN–NPOC relationship is compatible with a dynamic aerosol-processing framework, while the contribution of individual atmospheric processes, including regeneration-related processes, cannot be resolved from the present dataset because these processes were not directly measured.

CONCLUSIONS

This pilot study provides a preliminary characterization of $PM_{2.5}$ composition and potential source influences in urban Tirana using elemental analysis, water-soluble NPOC and TN measurements, Pearson correlation analysis and complementary atmospheric datasets. The 2024 campaign was characterized by higher crustal-associated elemental concentrations than 2025, while MERRA-2 and HYSPLIT results were consistent with a relatively stronger mineral dust influence during this period. Traffic-related elemental patterns were consistent with the possible influence of non-exhaust processes and resuspended road dust, whereas no clear evidence of a dominant industrial contribution was identified among the analyzed tracers. Marine-associated elements indicated a possible intermittent marine influence, although marine and non-marine contributions could not be clearly distinguished.

Moderate positive correlations between NPOC and TN were consistent with partially shared atmospheric behavior, while meteorological observations provided complementary environmental context rather than evidence of direct causal effects. Overall, the results provide an exploratory qualitative characterization rather than quantitative source apportionment. Differences between the two campaigns may also reflect their distinct sampling periods and meteorological conditions. Although exploratory, the integrated approach applied in this study may provide a preliminary framework for identifying potential source-related patterns that could be further evaluated in studies based on longer monitoring periods and larger datasets. In such studies, source-related hypotheses derived from elemental correlations and complementary atmospheric information could be compared with multivariate or receptor-model approaches, such as PCA or PMF, to assess whether similar source patterns are identified.

Acknowledgements

The authors gratefully acknowledge the Faculty of Natural Sciences, University of Tirana, for supporting this study and the Institute of Atmospheric Sciences and Clime (ISAC-CNR), Lecce, Italy, for providing laboratory facilities and analytical support.

REFERENCES

1. Ali, N., Kausar, A., Vambol, S., Kozub, P., Kozub, S., Hrynzovskyi, A. (2024). Environmental retrieval during COVID-19 lockdown in the megacity Karachi, Pakistan. *Ecological Questions, 35*(3), 1–16. https://doi.org/10.12775/EQ.2024.032
2. Amato, F., Cassee, F.R., Denier van der Gon, H.A.C., Gehrig, R., Gustafsson, M., Hafner, W., Harrison, R.M., Jozwicka, M., Kelly, F.J., Moreno, T., Prevot, A.S.H., Schaap, M., Sunyer, J. and Querol, X., 2014. Urban air quality: The challenge of traffic non-exhaust emissions. *Journal of Hazardous Materials, 275*, 31–36. https://doi.org/10.1016/j.jhazmat.2014.04.053
3. Amato, F., Pandolfi, M., Viana, M., Querol, X., Alastuey, A., Moreno, T. (2009). Spatial and chemical patterns of PM_{10} in road dust deposited in urban environment. *Atmospheric Environment, 43*(9), 1650–1659. https://doi.org/10.1016/j.atmosenv.2008.12.009
4. Analitis, A., Katsouyanni K., Dimakopoulou K., Samoli E., Nikoloulopoulos A.K., Petasakis Y., et al. (2006) Short-term effects of ambient particles on cardiovascular and respiratory mortality. *Epidemiolog,. 17*, 230– 3. https://doi.org/10.1097/01.ede.0000199439.57655.6b
5. Brown, S.S., Dubé, W.P., Tham, Y.J., Zha, Q., Xue, L., Poon, S., Wang, Z., Blake, D.R., Tsui, W., Parrish D.D., Wang, T. (2016). Nighttime chemistry at a high-altitude site above Hong Kong. *Journal of Geophysical Research: Atmospheres, 121*, 2457–2475.
6. Brown, S.S., Roberts, J.M., Dube, W.P., Thornton, J.A., Goldstein, A.H. (2006). Variability in nocturnal nitrogen oxide processing and its role in regional air quality. *Science 311*, 67–70.
7. Caushaj, M., Mandija, F., Keckhut, P., Alraddawi, D., Premti, D., Miço, S., Frasheri, N., Vila, F. (2026) Aerosols under heatwaves: Interactions between pollution and heatwave extremes. *EPJ Web of Conferences, 365*, 04004. https://doi.org/10.1051/epjconf/202636504004 (a)
8. Caushaj, M., Mandija, F., Premti, D., Dushku, S. (2026). Chemical characterization of $PM_{2.5}$ in the

urban air of Tirana: Sources, chemical markers and atmospheric secondary processes. *ICNTC Conference Proceedings Book 2026*. (b)

9. Çaushaj, M., Premti, D., Ylli, F., Pinguli, L., Manaj, H., Prifti, T., Malollari, I. (2024). Air pollution analysis and continuous monitoring of particulate matter (PM2.5) in an urban area. *Journal of Natural Sciences (JNS), 35*, 58–70
10. Caushaj, M., Mandija, F., Premti, D. (2026). Atmospheric chemical transformations, regeneration and transport: the invisible bridge enabling the integration of positive matrix factorisation, remote sensing, for air-quality assessment. *Preprints* 202607.1170, Version 1. https://doi.org/10.20944/preprints202607.1170.v1 (c)
11. Çela, G., Papathimiu, S., Kosovrasti, A., Halili, A., Laçi, S. (2026). Analyzing the landuse and landcover changing dynamics in the myzeqe plain of Albania, using GIS/RS, for the period 1991–2020. *Proceedings on Engineering Sciences 8*(1), 573–578. https://doi.org/10.24874/PES08.01B.021 Publisher: Faculty of Engineering, University of Kragujevac.
12. Copernicus. (2025). *Saharan dust affects Italy*. European Union, Copernicus Programme, Sentinel-3 imagery acquired 15 April 2025.
13. Ejaz, F., Kausar, A., Ulfat, I., Vambol, S., Vambol, V., Lyndiuk, O. (2026). Geospatial assessment of urban environmental and mitigation strategies for thermal stress in Lahore, Karachi, and Islamabad. *Applied Geomatics, 18*(3), 110. https://doi.org/10.1007/s12518-026-00759-2
14. Ervens, B., Turpin, B. J., and Weber, R. J. (2011). Secondary organic aerosol formation in cloud droplets and aqueous particles (aqSOA): a review of laboratory, field and model studies, *Atmos. Chem. Phys., 11*, 11069–11102, https://doi.org/10.5194/acp-11-11069-2011
15. Escudero, M., Querol, X., Àvila, A., Cuevas, E. (2007). Origin of the exceedances of the European daily PM limit value in regional background areas of Spain. *Atmospheric Environment, 41*(4), 730–744. https://doi.org/10.1016/j.atmosenv.2006.09.014
16. EUMETSAT. (2024). *Dust events in the Mediterranean in early 2024*. European Organisation for the Exploitation of Meteorological Satellites.
17. EUMETSAT. (2024). Dust transport from Sahara to Mediterranean and beyond. https://user.eumetsat.int/resources/case-studies/dust-transport-from-sahara-to-mediterranean-and-beyond
18. European Committee for Standardization (CEN). *EN 12341:2014—Ambient air: Standard gravimetric measurement method for the determination of the PM10 or PM2.5 mass concentration of suspended particulate matter*. Brussels, Belgium; 2014.
19. Finlayson-Pitts, B.J., Wingen, L.M., Sumner, A.L., Syomin, D., Ramazan, K.A. (2002). The heterogeneous hydrolysis of NO_2 in laboratory systems and in outdoor and indoor atmospheres: an integrated mechanism. *Physical Chemistry Chemical Physics 5*, 223–242.
20. Gaffney, J.S, Marley, A.N. (2005). The importance of the chemical and physical properties of aerosols in determining their transport and residence times in the troposphere, *Urban Aerosols and Their Impacts.*
21. Gelaro, R., McCarty, W., Suárez, M.J., et al. (2017). The modern-era retrospective analysis for research and applications, version 2 (MERRA-2). *Journal of Climate, 30*, 5419–5454.
22. Gietl, J.K., Lawrence, R., Thorpe, A.J., Harrison, R.M. (2010). Identification of brake wear particles and derivation of a quantitative tracer for brake dust at a major road. *Atmospheric Environment, 44*(2), 141–146. https://doi.org/10.1016/j.atmosenv.2009.10.016
23. Gietl, J.K., Lawrence, R., Thorpe, A.J., Harrison, R.M. (2010). Identification of brake wear particles and derivation of a quantitative tracer for brake dust at a major road. *Atmospheric Environment, 44*(2), 141–146. https://doi.org/10.1016/j.atmosenv.2009.10.016
24. Green, J.R., Fiddler, M.N., Holloway, J.S., Fibiger, D.L., McDuffie, E.E., Campuzano-Jost, P., et al. (2019). Rates of wintertime atmospheric SO2 oxidation based on aircraft observations during clear-sky conditions over the eastern United States. *Journal of Geophysical Research: Atmospheres, 124*, 6630–6649. https://doi.org/10.1029/2018JD030086
25. Griffith, E.C., Carpenter, B.K., Shoemaker, R.K., Vaida, V. (2013). *Photochemistry of aqueous pyruvic acid.* Proceedings of the National Academy of Sciences of the United States of America 110, 11714–11719.
26. Grigoratos, T., Martini, G. (2015). Brake wear particle emissions: A review. In: 14th EuCheMS International Conference on Chemistry and the Environment (ICCE 2013); 25 June 2013; Barcelona (Spain). *Environmental Science And Pollution Research 22*(4), 2491–2504. JRC92042.
27. Grigoratos, T., Martini, G. (2014). *Non-exhaust traffic related emissions: Brake and tyre wear PM*. Joint Research Centre, European Commission.
28. Grigoratos, T., Martini, G. (2015). Brake wear particle emissions: a review. *Environ Sci Pollut Res 22*, 2491–2504. https://doi.org/10.1007/s11356-014-3696-8
29. Hallquist, M., Wenger, J.C., Baltensperger, U., Rudich, Y., Simpson, D., Claeys, M., Dommen, J., Donahue, N.M., George, C., Goldstein, A. H., Hamilton, J.F., Herrmann, H., Hoffmann, T., Iinuma, Y.,

Jang, M., Jenkin, M.E., Jimenez, J.L., Kiendler-Scharr, A., Maenhaut, W., McFiggans, G., Mentel, Th.F., Monod, A., Prévôt, A.S.H., Seinfeld, J.H., Surratt, J.D., Szmigielski, R., and Wildt, J. (2009). The formation, properties and impact of secondary organic aerosol: current and emerging issues, *Atmos. Chem. Phys., 9*, 5155–5236, https://doi.org/10.5194/acp-9-5155-2009

30. Hallquist, M., Wenger, J.C., Baltensperger, U., Rudich, Y., Simpson, D., Claeys, M., Dommen, J., Donahue, N.M., George, C., Goldstein, A.H., Hamilton, J.F., Herrmann, H., Hoffmann, T., Iinuma, Y., Jang, M., Jenkin, M.E., Jimenez, J.L., Kiendler-Scharr, A., Maenhaut, W., McFiggans, G., Mentel, T., Monod, A., Pré vô t, A. S.H., Seinfeld, J.H., Surratt, J.D., Szmigielski, R., Wildt, J. (2009). Theformation, properties and impact of secondary organic aerosol: Currentand emerging issues. *Atmos. Chem. Phys. 9*, 5155−5236.
31. Hand, J.L. (2023). *IMPROVE Data User Guide 2023 (Version 2).* Interagency Monitoring of Protected Visual Environments (IMPROVE), 24 October 2023.
32. Hersbach, H., Bell, B., Berrisford, P., et al. (2020). The ERA5 global reanalysis. *Quarterly Journal of the Royal Meteorological Society, 146*, 1999–2049.
33. Hu, X., Chen, D., Hu, L., Li, B., Li, X., Fang, X. (2023). Global methyl halide emissions from biomass burning during 2003–2021. *Environmental Science and Ecotechnology 14*, 100228.
34. Hyslop, N.P., Trzepla, K., White, W.H. (2012). Reanalysis of archived IMPROVE PM2.5 samples previously analyzed over a 15-year period. *Environmental Science & Technology, 46*(18), 10106–10113. https://doi.org/10.1021/es301823q
35. Joutsensaari, J., Ozon, M., Nieminen, T., Mikkonen, S., Lähivaara, T., Decesari, S., Facchini, M., Laaksonen, A., Lehtinen, K.E.J. (2018). Identification of new particle formation events with deep learning. *Atmospheric Chemistry and Physics, 18*, 9597–9615. https://doi.org/10.5194/acp-18-9597-2018
36. Kulmala, M. (2003). How particles nucleate and grow. *Science 302*, 1000–1001.
37. Levy, R., Hsu, C., Sayer, A., Mattoo, S., Lee, J. (2017). *MODIS Atmosphere L2 Aerosol Product, Collection 6.1*. NASA MODIS Adaptive Processing System, Goddard Space Flight Center
38. Li, D., Li, Y., Li, G., Zhang, Y., Li, J., Chen, H. (2019). Fluorescent reconstitution on deposition of PM25 in lung and extrapulmonary organs. *Proc Natl Acad Sci USA. 116*, 2488–93. https://doi.org/10.1073/pnas.1818134116
39. Longfellow, C.A., Ravishankara, A.R., Hanson, D.R., Lovejoy, E.R. (2000). Reactive and nonreactive uptake on hydrocarbon soot. *Journal of Geophysical Research: Atmospheres 105*, 24345–24350.
40. Mandija, F., Caushaj, M., Premti, D., Keckhut, P., Alraddawi, D., Frasheri, N., Vila, F. (2025). Midlatitude spatial and temporal correlations between aerosol properties and weather extremes. *International Journal of Environment and Pollution, 75*(2), 110–132. https://doi.org/10.1504/IJEP.2025.148721
41. Monod, A., Sive, B.C. (2000). Aromatic hydrocarbons in urban air: Concentration and OH reactivity. *Environmental Science & Technology, 34*(22), 4821–4827.
42. Moreno, T., Querol, X., Castillo, S., Alastuey, A., Cuevas, E., Herrmann, L., Mounkaila, M., Elvira, J., Gibbons, W. (2006). Geochemical variations in aeolian mineral particles from the Sahara–Sahel dust corridor. *Chemosphere, 65*(2), 261–270. https://doi.org/10.1016/j.chemosphere.2006.02.052
43. Moreno, X.Q., Alastuey, A., García do Santos, S., Patier, R.F., Artiñano, B., Gibbons, W. (2006). PM source apportionment and trace metallic aerosol affinities during atmospheric pollution episodes: a case study from Puertollano, Spain. *J. Environ. Monit. 8*(10), 1060–1068. https://doi.org/10.1039/b608321h
44. Pacyna, J.M., Pacyna, E.G. (2001). An assessment of global and regional emissions of trace metals to the atmosphere from anthropogenic sources worldwide. *Environmental Reviews, 9*, 269–298. https://doi.org/10.1139/a01-012
45. Pan, S., Qiu, Y., Li, M., Yang, Z., Liang, D. (2022). Recent developments in the determination of PM2.5 chemical composition. *Bulletin of Environmental Contamination and Toxicology 108*, 819–823
46. Pant, P. and Harrison, R. (2013). Estimation of the contribution of road traffic emissions to particulate matter concentrations from field measurements: A review. *Atmospheric Environment, 77*, 78–97. https://doi.org/10.1016/j.atmosenv.2013.04.028
47. Papathimiu, S., Halili, A., Sula, F. (2026). GIS-based wildfire risk assessment in a mediterranean Protected Area: a multi-criteria analysis of Dajti National Park, Albania. https://doi.org/10.21163/gt_2026.213.02, Geographia Technica, published by: *Asociatia Geograhia Technica*, *21*(2), 16–32. http://dx.doi.org/10.21163/gt_2026.213.02
48. Pennetta, A., Bloise, E., Cesari, D., Deluca, G., Dinoi, A., Guascito, M.R., Merico, E., Potì, S., Semeraro, P., Unga, F., Contini, D. (2026). Comparison of techniques and measurement methods for determination of the water-soluble carbon and nitrogen in atmospheric particulate matter. *Microchem. J. 220*(116305).
49. Pey, J., Querol, X., Alastuey, A., Forastiere, F., and Stafoggia, M. (2013). African dust outbreaks over the Mediterranean Basin during 2001–2011: PM_{10} concentrations, phenomenology and trends,

and its relation with synoptic and mesoscale meteorology, *Atmos. Chem. Phys., 13*, 1395–1410, https://doi.org/10.5194/acp-13-1395-2013

50. Pitchford, M., Malm, W., Schichtel, B., Kumar, N., Lowenthal, D., Hand, J. (2007). Revised algorithm for estimating light extinction from IMPROVE particle speciation data, *Journal of the Air & Waste Management Association, 57*(11), 1326–1336,https://doi.org/10.3155/1047-3289.57.11.1326
51. Pons, F., Alberti, T., Messori, G., Dulac,F., Faranda, D. (2025). Assessingclimate change impacts on the March 2024 compound floods and Saharan dust outbreak in Europe. *Journal of Geophysical Research: Atmospheres, 130*, e2024JD042218. https://doi.org/10.1029/2024JD042218
52. Pope, C.A. and Dockery, D.W. (2006). Health effects of fine particulate air pollution: lines that connect, *Journal of the Air & Waste Management Association, 56*(6), 709–742. https://doi.org/10.1080/10473289.2006.10464485
53. Potì, S., Martina, L., Unga, F., Cesari, D., Dinoi, A., Pennetta, A., Bloise, E., Semeraro, P., Deluca, G., Cirillo Ciricugno, L., Giotta, L., Calcagnile, L., Mangone, A., Guascito, M.R., Contini, D. (2026). Unraveling the different drivers of $PM_{2.5}$ mass and oxidative potential at two sites of Southern Italy. *Environmental Science & Technology, 60*(22), 16044–16056. https://doi.org/10.1021/acs.est.6c02676
54. Premti, D., Hajdini, G., Caushaj, M., Manaj, H., Prifti, T., Pinguli, L., Malollari, I. (2026). $PM_{2.5}$ from wildfires as a potential phosphorus source for Lake Ohrid. *Ecological Engineering & Environmental Technology, 27*(3), 111–120. https://doi.org/10.12912/27197050/217107
55. Putaud, J., Raes, F., Van Dingenen, R., Brueggemann, E., Facchini, M., Decesari, S., Fuzzi, S., Gehrig, R., Hueglin, C., Laj, P., Lorbeer, G., Maenhout, W., Mihalopoulos, N., Mueller, K., Querol, X., Rodriguez, S., Schneider, J., Spindler, G., Ten Brink, H., Toerseth, K., Wiedensohler, A. (2004). A European aerosol phenomenology. Part 2: chemical characteristics of particulate matter at kerbside, urban, rural and background sites in Europe. *Atmospheric Environment 3,* 2579–2595. JRC27002.
56. Querol, X., Viana, M., Alastuey, A., Amato, F., Moreno, T., Castillo, S., Pey, J., de la Rosa, J., Sánchez de la Campa, A., Artíñano, B., Salvador, P., García Dos Santos, S., Fernández-Patier, R., Moreno-Grau, S., Negral, L., Minguillón, M.C., Monfort, E., Gil, J.I., Inza, A., Ortega, L.A., Santamaría, J.M., Zabalza, J. (2007). Source origin of trace elements in PM from regional background, urban and industrial sites of Spain. *Atmospheric Environment*, *41*(34), 7219–7231. https://doi.org/10.1016/j.atmosenv.2007.05.022
57. Rodríguez, S., Querol, X., Alastuey, A., Kallos, G., Kakaliagou, O. (2001). Saharan dust contributions to PM10 and TSP levels in Southern and Eastern Spain. *Atmospheric Environment, 35*, 2433–2447.
58. Seinfeld, J.H., Pandis, S.N. (2016). *Atmospheric Chemistry and Physics: From Air Pollution to Climate Change*. 3rd ed. Hoboken, NJ: Wiley.
59. Stein, A.F., Draxler, R.R., Rolph, G.D., Stunder, B.J.B., Cohen, M.D., Ngan, F. (2015). NOAA's HYSPLIT atmospheric transport and dispersion modeling system. *Bulletin of the American Meteorological Society, 96*(12), 2059–2077.
60. Streets, D.G., Bond, T.C., Carmichael, G.R., Fernandes, S.D., Fu, Q., He, D., Klimont, Z., Nelson, S.M., Tsai, N.Y., Wang, M.Q., Woo, J.H., Yarber, K.F. (2003). An inventory of gaseous and primary aerosol emissions in Asia in the year 2000. *Journal of Geophysical Research 108*, 8809.
61. Su, B., Wang, T., Zhang, G., Liang, Y., Lv, C., Hu, Y., Li, L., Zhou, Z., Wang, X., Bi, X. (2022). A review of atmospheric aging of sea spray aerosols: Potential factors affecting chloride depletion. *Atmospheric Environment, 290*, 119365. https://doi.org/10.1016/j.atmosenv.2022.119365
62. Thorpe, A., Harrison, R.M., (2008). Sources and properties of non-exhaust particulate matter from road traffic: A review, *Science of The Total Environment, 400*(1–3), 270–282, https://doi.org/10.1016/j.scitotenv.2008.06.007(https://www.sciencedirect.com/science/article/pii/S004896970800658X)
63. Tomasi, C. and Lupi, A. (2017). *Coagulation, Condensation, Dry and Wet Deposition, and Cloud Droplet Formation in the Atmospheric Aerosol Life Cycle*. In Atmospheric Aerosols (eds C. Tomasi, S. Fuzzi and A. Kokhanovsky). https://doi.org/10.1002/9783527336449.ch3
64. U.S. Environmental Protection Agency. (1999). *Compendium method IO-3.5: Determination of metals in ambient particulate matter using inductively coupled plasma/mass spectrometry (ICP/MS).* Research Triangle Park, NC: U.S. EPA.
65. Unga, F., Calzolai, G., Chiari, M., Cuccia, E., Colombi, C., Franciosa, M., Dinoi, A., Merico, E., Pennetta, A., Gómez-Sánchez, N., Mapelli, C., Pareti, S., Perrino, C., Yubero, E., Contini, D. (2025). Determination of aerosol composition by ED-XRF on teflon and quartz substrates: Potentialities and limits. *Aerosol Research, 3*, 405.
66. Viana, M., Kuhlbusch, T.A.J., Querol, X., Alastuey, A., Harrison, R.M., Hopke, P.K., Winiwarter, W., Vallius, M., Szidat, S., Prevot, A.S.H., Hueglin, C., Bloemen, H., Wahlin, P., Zecchi, R., Kasper-Giebl, A., Maenhaut, W., Hitzenberger, R. (2008). Source apportionment of particulate matter in Europe: A review of methods and results. *Journal of Aerosol Science 39*(10) 827–849. https://doi.org/10.1016/j.jaerosci.2008.05.007

67. Vicars, W.C., and Sickman, J.O. (2011), Mineral dust transport to the Sierra Nevada, California: Loading rates andpotential source areas, *J. Geophys. Res., 116*, G01018, https://doi.org/10.1029/2010JG001394
68. Wei-wei, W. (2009). Relationship between meteorological conditions and particle size distribution of atmospheric aerosols. *Journal of Meteorology and Environment*.
69. Winterbottom, C.J., Shah, R.J., Patterson, K.C., Kreider, M.E., Panettieri, R.A. Jr., Rivera-Lebron, B., et al. (2018). Exposure to ambient particulate matter is associated with accelerated functional decline in idiopathic pulmonary fibrosis. *Chest. 153*, 1221–8. https://doi.org/10.1016/j.chest.2017.07.034
70. Zanobetti, A., Franklin, M., Koutrakis, P., Schwartz, J. (2009). Fine particulate air pollution and its components in association with cause-specific emergency admissions. *Environ Health. 8*, 58. https://doi.org/10.1186/1476-069X-8-58
71. Zhang, R., Khalizov, A., Wang, L., Hu, M., Xu, W. (2012). Nucleation and growth of nanoparticles in the atmosphere. *Chemical Reviews, 112*, 1957–2011.
72. Zhang, R., Wang, G., Guo, S., Zamora, M.L., Ying, Q., Lin, Y., Wang, Y. (2015). Formation of urban fine particulate matter. *Chemical Reviews, 115*, 3803–3855.